Research Paper

GEOSPHERE

GEOSPHERE

https://doi.org/10.1130/GES02868.1

13 figures; 1 set of supplemental files

CORRESPONDENCE: zoe.molitor@yale.edu

CITATION: Molitor, Z., Jagoutz, O., Moser, A., Cruz-Uribe, A., and Cross, A., 2025, Permo-Carboniferous crustal structure and state of strain in the New England Appalachians, USA: Geosphere, https://doi.org/10.1130/GES02868.1.

Science Editor: Christopher J. Spencer
Associate Editor: Michael L. Williams

Received 14 February 2025
Revision received 6 August 2025
Accepted 28 August 2025

Published online 26 September 2025

Permo-Carboniferous crustal structure and state of strain in the New England Appalachians, USA

Z. Molitor[1], O. Jagoutz[2], A. Moser[2,*], A. Cruz-Uribe[3], and A. Cross[4]

[1]Yale University, Earth and Planetary Science Department, New Haven, Connecticut 06511, USA
[2]Massachusetts Institute of Technology, Department of Earth Atmospheric and Planetary Sciences, Cambridge, Massachusetts 02139, USA
[3]University of Maine, School of Earth and Climate Sciences, Orono, Maine 04469, USA
[4]Woods Hole Oceanographic Institution, Falmouth, Massachusetts 02543, USA

ABSTRACT

The Permo-Carboniferous Alleghanian orogeny is thought to represent the final collision of Laurasia and Gondwana in the Late Carboniferous and early Permian. Yet, in comparison to the prior Acadian (Devonian) and Taconic (Ordovician) orogenies, the spatio-temporal distribution of deformation and metamorphism in the Appalachian Mountains (eastern USA and Canada) relating to the Alleghanian orogeny remains enigmatic. Notably, there are very few direct constraints on fabric formation related to proposed Permo-Carboniferous shear zones outside of the Honey Hill–Lake Char fault system. Here, we present a compilation of macrostructural observations, new microstructural observations, and new in situ geochronology and geochemical data of monazite and titanite to constrain the distribution of Permo-Carboniferous deformation and metamorphism across the entire New England Appalachians (USA) while placing explicit constraints on fabric formation ages. Our findings suggest that Permo-Carboniferous deformation and metamorphism in the northern New England Appalachians (Vermont, New Hampshire, and Maine) are characteristic of upper crustal conditions (<15 km depth). Deformation in northern New England was defined by localized steep strike-slip shear zones bounding a semi-rigid to rigid medial block, the Central Maine terrane. In southern New England (south-central Massachusetts and Connecticut), the context and grade of Permo-Carboniferous metamorphism transitions from retrograde greenschist facies to prograde amphibolite facies. Corresponding to this change in metamorphic grade, the deformation style also changes. Northward extrusion in the northernmost New England Appalachians at greenschist facies conditions during retrograde metamorphism transitions to southeastward extrusion in the southernmost New England Appalachians at amphibolite facies conditions during prograde metamorphism. These observations suggest that one of two regimes controls Permo-Carboniferous structural and metamorphic style in the northern Appalachians: (1) zipper tectonics and extrusion in the Permo-Carboniferous due to continental collision or (2) gravitational collapse and upper crustal extrusion of an overthickened orogenic plateau such as the "Acadian altiplano".

Zoe Molitor https://orcid.org/0000-0003-0606-4323
Now at: Geosciences Department, Hamilton College, 198 College Hill Rd, Clinton, NewYork 13323, USA

1. INTRODUCTION

The Appalachian orogen in the United States preserves a protracted record of orogenesis from ca. 500 Ma to 250 Ma (Bird and Dewey, 1970; Robinson et al., 1998; van Staal et al., 2009). In the New England Appalachian Mountains, this includes the Taconic (Macdonald et al., 2014; Karabinos et al., 2017; Valley et al., 2020), Salinic (van Staal et al., 2009), Acadian and Neoacadian (Robinson et al., 1998; van Staal et al., 2009; Massey et al., 2017; Hillenbrand et al., 2021), and Alleghanian (Wintsch et al., 1992) orogenies. The extent of Alleghanian metamorphism and deformation in the New England Appalachians and its relationship to the plate kinematic and geodynamic regime in the late Paleozoic have long been a subject of discussion (Wintsch and Sutter, 1986; Wintsch et al., 1992, 2003, 2014; Faure et al., 1996; Moecher, 1999). While early workers hypothesized that distributed Alleghenian tectonism was limited to southernmost New England (e.g., Murray, 1988), a growing body of literature over the last few decades has established Permo-Carboniferous, nominally Alleghanian-age metamorphism and deformation along the Bronson Hill anticlinorium in western New Hampshire (Harrison et al., 1989; Spear et al., 2008; Massey and Moecher, 2013; McWilliams et al., 2013), in southeastern Maine along the Norumbega fault system (West and Lux, 1993), and proximal to the Sebago batholith located in southwestern Maine (Tomascak et al., 1996; Walters et al., 2022; see also Fig. 1). Of particular interest is the observation of Late Carboniferous sinistral shear along the Bronson Hill anticlinorium (Massey and Moecher, 2013; McWilliams et al., 2013), contemporaneous with dextral shear on the Norumbega fault system (West and Lux, 1993) during the early Alleghanian orogeny (ca. 330–300 Ma). A kinematic model for the Alleghanian orogeny must reconcile these contrasting shear senses in the north and central New England Appalachians with pervasive NW-SE-directed early Alleghanian deformation documented in eastern Connecticut (Wintsch and Sutter, 1986).

Early models inferred that the orientations of bedrock structures can be directly related to the principal stress orientations and therefore the plate convergence direction. For example, the rotation of strikes of the foliation plane in eastern Connecticut and conflicting senses of shear along Permo-Carboniferous shear zones have been explained through a rotation of the

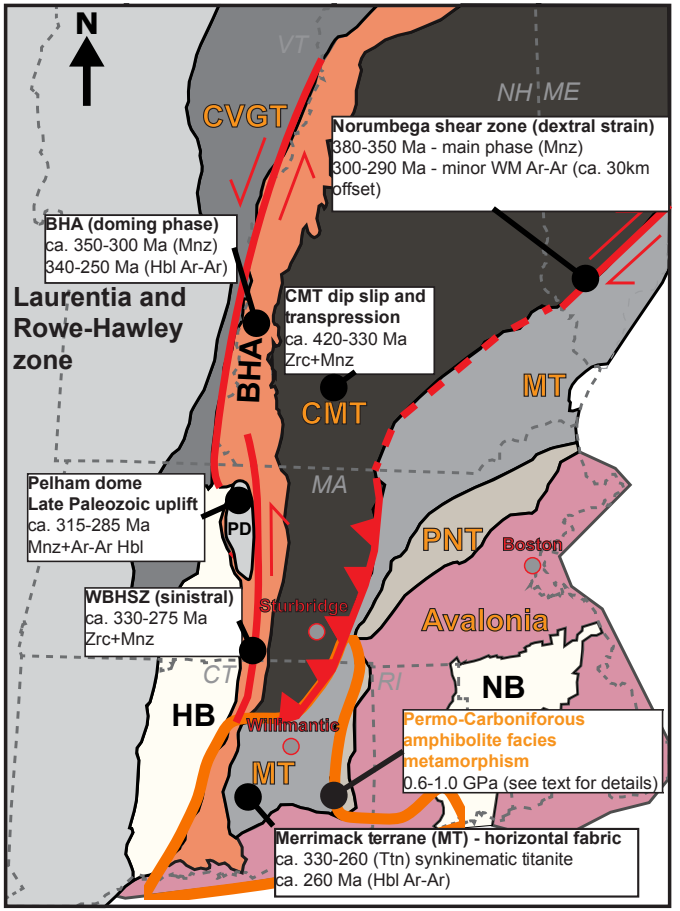

Figure 1. Simplified geological map of New England, USA, with a focus on major episodes of Permo-Carboniferous deformation and metamorphism recognized in the literature (modified from Aleinikoff et al., 2007). Published age constraints for major shear zones and internal deformation of terranes are given in associated white boxes. Age constraints for Norumbega shear zone are from West and Lux (1993) and Gerbi and West (2007). Ages for Bronson Hill anticlinorium (BHA) are from Spear et al. (2008; monazite [Mnz] U-Pb) and Wintsch et al. (2003; Ar-Ar). Ages for Central Maine terrane (CMT) are from Moecher et al. (2021), and Western Bronson Hill shear zone (WBHSZ) from Massey et al. (2017) and McWilliams et al. (2013). Ages for Pelham dome (PD) are from Hillenbrand et al. (2023a). CVGT—Connecticut Valley Gaspé trough; HB—Hartford Basin; MT—Merrimack Terrane; PNT—Putnam-Nashoba Terrane; NB—Narrangansett Basin; Hbl—hornblende; Ttn—titanite; Zrc—zircon; WM—white mica. Region of Permo-Carboniferous amphibolite facies metamorphism is based on Moecher and Wintsch (1994), Murray (1988), Wintsch et al. (2003), and Fetherston et al. (2014). State boundaries are presented as dashed lines in background with two-letter state abbreviations: CT—Connecticut; MA—Massachusetts; ME—Maine; NH—New Hampshire; RI—Rhode Island; VT—Vermont. Select major cities, referenced in text or of geographical significance, are shown.

convergence direction, typically in the Permian (e.g., multistage models of Wintsch and Sutter, 1986, and Sacks and Secor, 1990). Indeed, there is a robust record of variations in the local Alleghanian stress field from the Narragansett Basin and Honey Hill–Lake Char fault system (e.g., Wintsch and Sutter, 1986; Rich, 2006). However, variations in the local principal stress direction need not translate directly to the convergence direction in regions where the plate boundary is oriented oblique to the convergence direction (e.g., Tikoff and Teyssier, 1994; Chang et al., 2003; Dayem et al., 2009). Additionally, there exist very few data that directly constrain the absolute timing of these deformation episodes with modern, in situ geochronologic techniques. It is possible that significant variations in the stress direction at a regional scale resulted from a strongly oblique collision with near-constant convergence direction (i.e., single-stage collision; e.g., Vauchez et al., 1987; Hatcher, 2002).

In this work, we investigate the structure and timing of Permo-Carboniferous deformation in eastern Connecticut. We present a synthesis of previously collected bedrock structure data compiled from existing bedrock geologic maps of eastern Connecticut. We pair these data with new observations of macro- and microscopic shear sense indicators as well as new in situ monazite and titanite geochronologic constraints on the timing of distributed Alleghanian deformation and Alleghanian fabric formation in eastern Connecticut.

2. GEOLOGIC BACKGROUND AND OVERVIEW OF EXISTING GEOCHRONOLOGY

The New England Appalachians record Paleozoic orogenesis spanning ca. 500–250 Ma, culminating in the formation of Pangea following closure of the Rheic Ocean. This orogenesis can be subdivided into three major episodes: the Taconic orogeny (ca. 500–445 Ma; Aleinikoff et al., 2002; Macdonald et al., 2014; Karabinos et al., 2017; Valley et al., 2020), the Acadian orogeny (ca. 420–395 Ma; van Staal et al., 2009; Massey et al., 2017; Hillenbrand et al., 2021), and the Alleghanian orogeny (ca. 330–275 Ma; Wintsch and Sutter, 1986; Wintsch et al., 1992) (complete history simplified from Robinson et al., 1998). Evidence also exists for intermediate orogenic events between each major episode including the Salinic orogeny (ca. 450–423 Ma; van Staal et al., 2009) and the Neoacadian orogeny (ca. 395–350 Ma; Robinson et al., 1998; van Staal et al., 2009; Waldron et al., 2022; Hillenbrand et al., 2023a, 2023b). In this work, we use "Neoacadian orogeny" to refer specifically to the episode of Late Devonian metamorphism and deformation observed in the New England Appalachians (e.g., Robinson et al., 1998), without addressing the involvement of the Meguma terrane (Waldron et al., 2022). Continental rifting began in the Triassic (Schlische, 1993), followed by continental breakup and the formation of the Atlantic Ocean basin starting at ca. 200 Ma (Blackburn et al., 2013; Davies et al., 2017; Withjack et al., 2020; Kinney et al., 2022).

Our understanding of Permo-Carboniferous, nominally "Alleghanian", deformation and metamorphism in the New England Appalachians derives largely from studies of central and eastern Connecticut (e.g., Wintsch, 1979; O'Hara,

1986; Wintsch and Sutter, 1986; Goldstein, 1989; Getty and Gromet, 1992; Sevigny and Hanson, 1993; Wintsch et al., 1992, 2007, 2014, 2024; Moecher and Wintsch, 1994; Moecher et al., 1997; Moecher, 1999; Aleinikoff et al., 2002, 2007; Walsh et al., 2007, 2021; Growdon et al., 2013). Many of these studies targeted major shear zones such as the shear zone around Willimantic dome and the likely correlative Honey Hill–Lake Char fault zone (Wintsch, 1979; Goldstein, 1989; Getty and Gromet, 1992; Moecher and Wintsch, 1994; Moecher, 1999). These investigations reveal significant Permo-Carboniferous top-to-the-NW extension along these structures, beginning under amphibolite facies conditions and continuing through the cataclastic field around the brittle-ductile transition (Wintsch, 1979; Getty and Gromet, 1992). Much of this extensional deformation occurred during the Permian as opposed to the Carboniferous based on titanite crystallization ages of ca. 300–290 Ma (Getty and Gromet, 1992; Wintsch et al., 1992). However, with particular regard to the Merrimack Terrane, southernmost Central Maine terrane, and parts of Avalonia and Ganderia, it is uncertain whether or not there was pervasive metamorphism and deformation preceding top-to-the-NW deformation on major shear zones but postdating prior Early to Middle Devonian metamorphism associated with the Acadian-Neoacadian orogeny.

During the Late Devonian and Permo-Carboniferous—prior to and during deformation around Willimantic dome and on the Honey Hill–Lake Char fault system—many gneiss domes in New England experienced exhumation, retrograde metamorphism, and significant deformation of metasedimentary and metavolcanic dome cover. Prominent and well-studied examples of these domes include Pelham dome (Wintsch et al.,1992; Moecher, 1999; Kim and Bell, 2005; Hillenbrand et al., 2023a) and Taconic (Oliverian) domes in the Bronson Hill anticlinorium (Harrison et al., 1989; Spear and Harrison, 1989; Wintsch et al., 1992; Walsh et al., 2007; Spear et al., 2008; Hillenbrand et al., 2021, 2023a). Additionally, Waterbury dome displays evidence for Early to Late Carboniferous exhumation and cooling (Hillenbrand et al., 2023b). Pelham dome, the Bronson Hill anticlinorium, and much of central-eastern Connecticut are defined by Permo-Carboniferous Ar-Ar mineral cooling ages (hornblende: 500 °C; muscovite: 400 °C; biotite: 300 °C; and K-feldspar: ~250 °C), suggesting Permo-Carboniferous cooling from prior, Late Devonian or Early Mississippian amphibolite facies conditions (Harrison et al., 1989; Spear and Harrison, 1989; Hillenbrand et al., 2021). In central Massachusetts, particularly around Pelham dome, petrochronologic evidence suggests that the Permo-Carboniferous was a time of retrogradation, increased deformation partitioning, and orogenic collapse (Massey et al., 2017; Hillenbrand et al., 2021, 2023a). However, it is not clear that this was the case for eastern Connecticut, particularly in regard to the Merrimack Terrane and Willimantic dome, which are both much farther east than the Bronson Hill anticlinorium and Pelham dome.

In the Late Carboniferous, a conjugate strike-slip shear system developed on the margins of the Central Maine terrane (Fig. 1). A sinistral shear zone, termed the Western Bronson Hill shear zone, is documented from central Massachusetts to central Vermont (Massey and Moecher, 2013; McWilliams et al., 2013). Meanwhile, the contemporaneous dextral Norumbega shear zone extended across coastal Maine, possibly continuing through southeastern New Hampshire or outboard of the coastline in New Hampshire and Massachusetts (e.g., West and Lux, 1993; West and Hubbard, 1997; Wang and Ludman, 2003; Kuiper, 2016). Similar Carboniferous dextral shear zones are observed in the Maritimes Basin in Canada (Waldron et al., 2015), along the Brevard fault zone in the southern Appalachians (Vauchez, 1987; Hatcher, 2001), and on the margins of the Mesetta block in Morocco (Houari and Hoepffner, 2003). Additionally, there are well-documented Late Devonian to Carboniferous dip-slip faults in eastern Connecticut on the margins of the Merrimack Terrane (Fig. 1; Rodgers, 1985). The Carboniferous strike-slip deformation coincides with gneiss dome formation and cooling of the Central Maine terrane and Bronson Hill in central and northern New England (Massey and Moecher, 2013; McWilliams et al., 2013). It was also contemporaneous with prograde Permo-Carboniferous metamorphism of the Narragansett Basin and Avalonia in southern New England (Murray, 1988; Fetherston et al., 2014).

Existing work suggests that the Merrimack Terrane experienced a similar episode of Permo-Carboniferous prograde metamorphism to the Narragansett Basin, albeit more so during the Carboniferous as opposed to the Permian. The internal deformation and metamorphism of the Merrimack Terrane (including metasedimentary lithologies such as the Hebron Formation and Scotland Schist) are, by comparison to its bounding shear zones (i.e., the Honey Hill–Lake Char fault system, the Willimantic fault, and faults within the Tatnic Hill Formation), poorly understood. Wintsch et al. (2007) applied zircon, monazite, and titanite geochronology to study the Hebron Formation, Devonian felsic gneisses, and neighboring Tatnic Hill Formation in eastern Connecticut. The study found that the metasedimentary units (the Hebron Formation and Tatnic Hill Formation) were deposited in the latest Ordovician through Silurian. The study also found many of the large felsic orthogneiss units within the Merrimack Terrane (i.e., Eastford and Canterbury Gneisses) intruded the section in the Early to Middle Devonian. Intrusion of these gneisses was followed by at least one episode of Carboniferous recrystallization at ca. 300 Ma (Wintsch et al., 2007). Another study by Walsh et al. (2021) attempted to constrain the chronology of deposition, tectonism, and metamorphic events in the neighboring Putnam-Nashoba terrane and Tatnic Hill belt (Fig. 1; also termed the Quinebaug-Marlboro belt). Walsh et al. identified Carboniferous deformation and decompression melting within the belt in south-central Massachusetts (ca. 340–320 Ma) contemporaneous with regional exhumation.

A general increase in Alleghanian metamorphic grade is documented from north to south in New England, most notably along the Bronson Hill anticlinorium (Wintsch et al., 2003) and within the Narragansett Basin (Murray, 1988). In northern New England (New Hampshire and Vermont), Alleghanian greenschist facies metamorphism is documented along the Bronson Hill anticlinorium (McWilliams et al., 2013) and Norumbega shear zone. There is no evidence for regionally extensive, prograde Alleghanian metamorphism within the Central Maine terrane (excluding relatively localized metamorphism around the Sebago batholith) or Merrimack Terrane in New Hampshire and Maine.

Given all of this previous work, there are several outstanding questions about Permo-Carboniferous deformation in southern New England:

(1) Was all Permo-Carboniferous metamorphism and deformation in southern New England a manifestation of regional orogenic collapse (i.e., localization of strain, exhumation, and cooling), or was there a distinct phase of Carboniferous prograde metamorphism (i.e., burial) outside of the Narragansett Basin and parts of Avalonia?

(2) How did regional conjugate strike-slip shear traverse southern New England, and does its structure and kinematic history better reflect gravitational collapse and lateral escape or compression-induced extrusion at a regional scale?

(3) Is there a distinct change in deformation style associated with the observed change in Alleghanian metamorphic grade in southern New England as compared to northern New England?

3. METHODS

3.1 Structural Data and Microstructural Analysis

To address the outstanding questions about Permo-Carboniferous deformation, we present a new compilation of macrostructural data for the southern New England Appalachians in southern New Hampshire, central Massachusetts, and eastern Connecticut (Fig. 2). The macrostructural data are compiled from existing bedrock geologic maps in the region as well as new supplemental fieldwork, including measurements of foliation, mineral lineation, and fold hinge lineation for the dominant structures. These data are plotted both on maps, using ArcGIS Pro software, and on stereonets, using the Orient program (Vollmer, 1990, 1995, 2024). For Figure 2, the foliation data are binned into an arbitrary 40 × 40 grid (~2.5 × 2.5 km spacing) across eastern Connecticut. For each "box" within

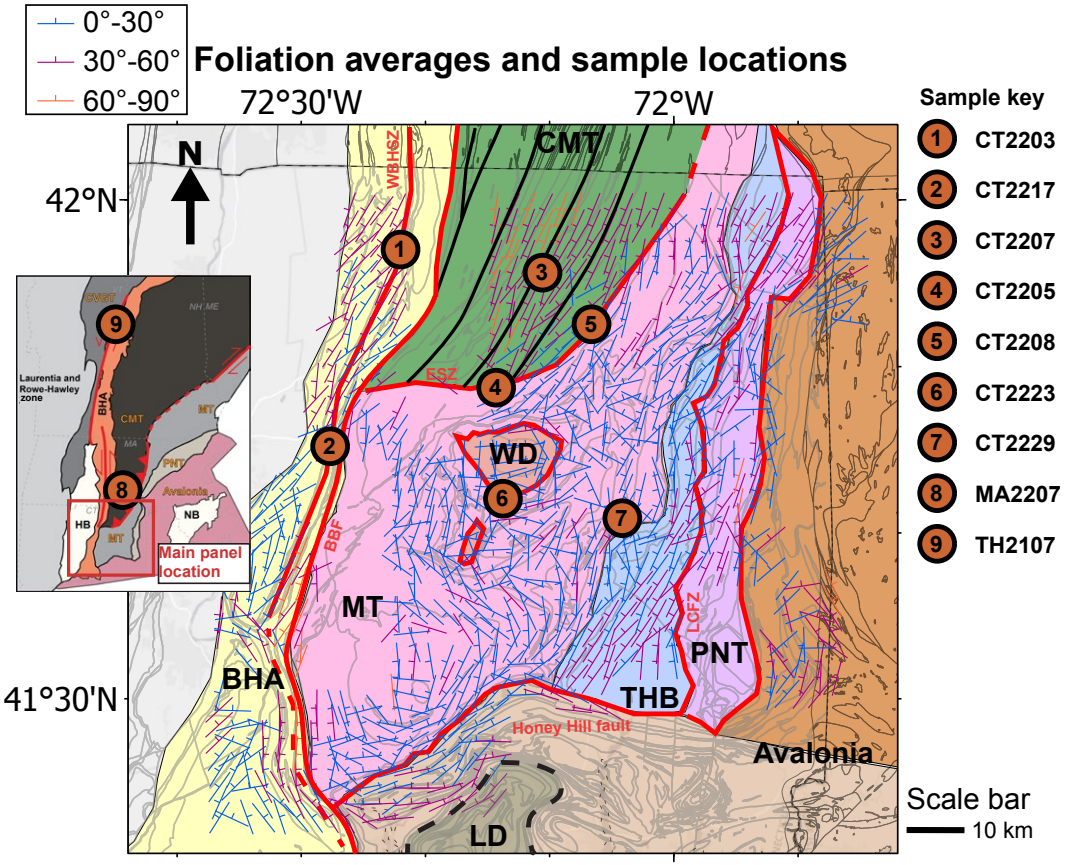

Figure 2. Compiled macroscopic foliation data from Connecticut and Massachusetts bedrock geologic maps. Sample locations discussed in text are shown with orange circles. Compiled foliations are averaged into a 40 × 40 grid (2.5 × 2.5 km) for visualization. Individual measurements are available in Table S2 (see text footnote 1). Foliation averages for each grid point are colored by dip magnitude in 30° increments. Acronyms are the same as in Figure 1 except: BBF—Bonemill Brook fault; ESZ—Eastford shear zone; LCFZ—Lake Char fault zone; LD—Lyme dome; THB—Tatnic Hill belt; WD—Willimantic dome. Bedrock data references: Collins (1954), Aiken (1955), Herz (1955), Snyder (1961, 1964a, 1964b, 1967, 1970), Dixon (1965, 1968, 1974, 1982), Dixon and Shaw (1965), Feininger (1965), Dixon and Pessl (1966), Lundgren and Ashmead (1966), Goldsmith (1967a, 1967b), Harwood and Goldsmith (1971), Lundgren et al. (1971), Eaton and Rosenfeld (1972), Pease (1972, 1988), Peper and Pease (1975), Fahey and Pease (1977), Lundgren (1979), Moore (1983), Dixon and Felmlee (1986), and Deasy and Wintsch (2019).

the grid, a representative foliation orientation is determined by conducting eigenvector analysis on the entire set of data within the box. The orientation corresponding to the maximum eigenvector-eigenvalue pair of the data within the box is shown. This orientation corresponds roughly to the "average" orientation of the foliation within the box (see Vollmer, 1990, 2024, for details on the eigenvector analysis and subdomain binning method, respectively).

For microstructural analysis, we cut two mutually perpendicular, oriented sections perpendicular to the foliation plane. If a macroscopic lineation was present, the two sections were cut parallel and perpendicular to the lineation. We assessed both sections for asymmetric shear sense indicators to investigate the relative roles of dip-slip, strike-slip, and pure shear deformation in each sample. Sample locations are shown in Figure 2 and made available in Table S1.[1] The macrostructural data referenced in this work are available in Table S2.

3.2 Electron Microprobe (EPMA) X-Ray Mapping

To characterize compositional zonation and inform spot placement during in situ laser ablation–inductively coupled plasma–mass spectrometry (LA-ICP-MS) analysis, we produced compositional maps of selected late-kinematic monazite and synkinematic titanite in four samples. Backscattered electron (BSE) images and elemental X-ray maps from wavelength dispersive spectrometry (WDS) were obtained using a JEOL 8200 electron probe microanalyzer (EPMA) at the Massachusetts Institute of Technology. For monazite, we produced elemental maps of Ca, Ce, Th, and Y, whereas for titanite, we produced elemental maps of Al, Ce, Fe, and Nb (see section 4). WDS map conditions are available in Table S3.

3.3 Laser Ablation–Inductively Coupled Plasma–Mass Spectrometry (LA-ICP-MS)

We obtained U-Pb dates to provide geochronologic constraints on the age of deformation (i.e., fabric ages) and metamorphism in proximity to the Eastford shear zone and throughout the Merrimack Terrane and Willimantic dome. In situ titanite and monazite isotope and trace element compositions were determined by LA-ICP-MS at the University of Maine MicroAnalytical Geochemistry and Isotope Characterization (MAGIC) laboratory. Trace element and U-Pb data were collected using an ESI NWR193UC excimer laser ablation system coupled to an Agilent 8900 inductively coupled plasma–mass spectrometer following Walters et al. (2022). The isotope ratio and trace element data are available in Tables S4–S7. Additional LA-ICP-MS methodology including discussion of standards, handling of errors, and monazite and titanite workflow is included in Supplemental Text S1.

To constrain the approximate temperature of metamorphism and subsequent deformation, we calculated zirconium (Zr)–in–titanite temperatures (Hayden et al., 2008). This thermometer requires constraints on pressure, TiO_2 and SiO_2 activities, and Zr contents in the crystal. All the samples containing titanite also contained quartz as a major phase, and therefore we assume that $a_{(SiO2)} = \sim 1$ (where a is activity). Rutile is not an equilibrium phase with titanite in our samples, and therefore we assume $a_{(SiO2)} = \sim 0.75 \pm 0.25$ (Ghent and Stout, 1984; Kapp et al., 2009; Chambers and Kohn, 2012). The pressure during titanite growth during Alleghanian metamorphism is the largest uncertainty in calculating titanite crystallization temperatures. Previous studies on Alleghanian metamorphism in eastern Connecticut suggest pressures of metamorphism of 0.7 ± 0.3 GPa (Moecher and Wintsch, 1994; Moecher, 1999; Wintsch et al., 2003). We ascribe a relatively large uncertainty to these pressure estimates due to the lack of sample coverage and detailed petrogenetic modeling.

3.4 Electron Backscatter Diffraction (EBSD)

To assess the effect of crystal-plastic deformation on titanite isotopic compositions and therefore titanite dates (e.g., Moser et al., 2022), we collected new electron backscatter diffraction (EBSD) maps of the same titanite grains dated by LA-ICP-MS. We utilized a variable pressure mode at 40 Pa (as opposed to carbon coating) to prevent charging during EBSD analysis. EBSD data were collected at the Marine Biological Laboratory (Woods Hole, Massachusetts) using a Zeiss Supra 40VP field emission gun scanning electron microscope equipped with an Oxford Instruments Symmetry EBSD detector. EBSD maps were collected at 30 kV accelerating voltage and 70° sample tilt. The working distance and step size of each analysis was dependent on the size and position of each grain within the section. A table of the working distance and step size for each grain map is available in Table S3. EBSD data postprocessing was conducted in the open-source MTEX toolbox for MATLAB (Bachmann et al., 2010).

4. RESULTS

4.1 Central Maine Terrane

4.1.1 Macro- and Microstructural Observations

Much of the internal structure of the Central Maine terrane reflects Acadian-Neoacadian deformation prior to the Alleghanian orogeny (Eusden and Barrerio, 1988; Eusden and Lyons, 1993; Robinson et al., 1998; Massey and Moecher, 2013; Massey et al., 2017; Hillenbrand et al., 2021, 2023a; Moecher et al., 2021). Foliations within the Central Maine terrane of northeastern Connecticut are steeply to moderately west dipping, whereas both mineral lineations and fold axes are subhorizontal and north-south trending (Figs. 2 and 3). The Late Devonian metamorphic assemblages in central Massachusetts and northeastern

[1]Supplemental Material. Supplemental Text S1–S3 and Figures S1–S16; Tables S1–S7 are available as separate Microsoft Excel files. Please visit https://doi.org/10.1130/GEOS.S.30056083 to access the supplemental material, and contact editing@geosociety.org with any questions.

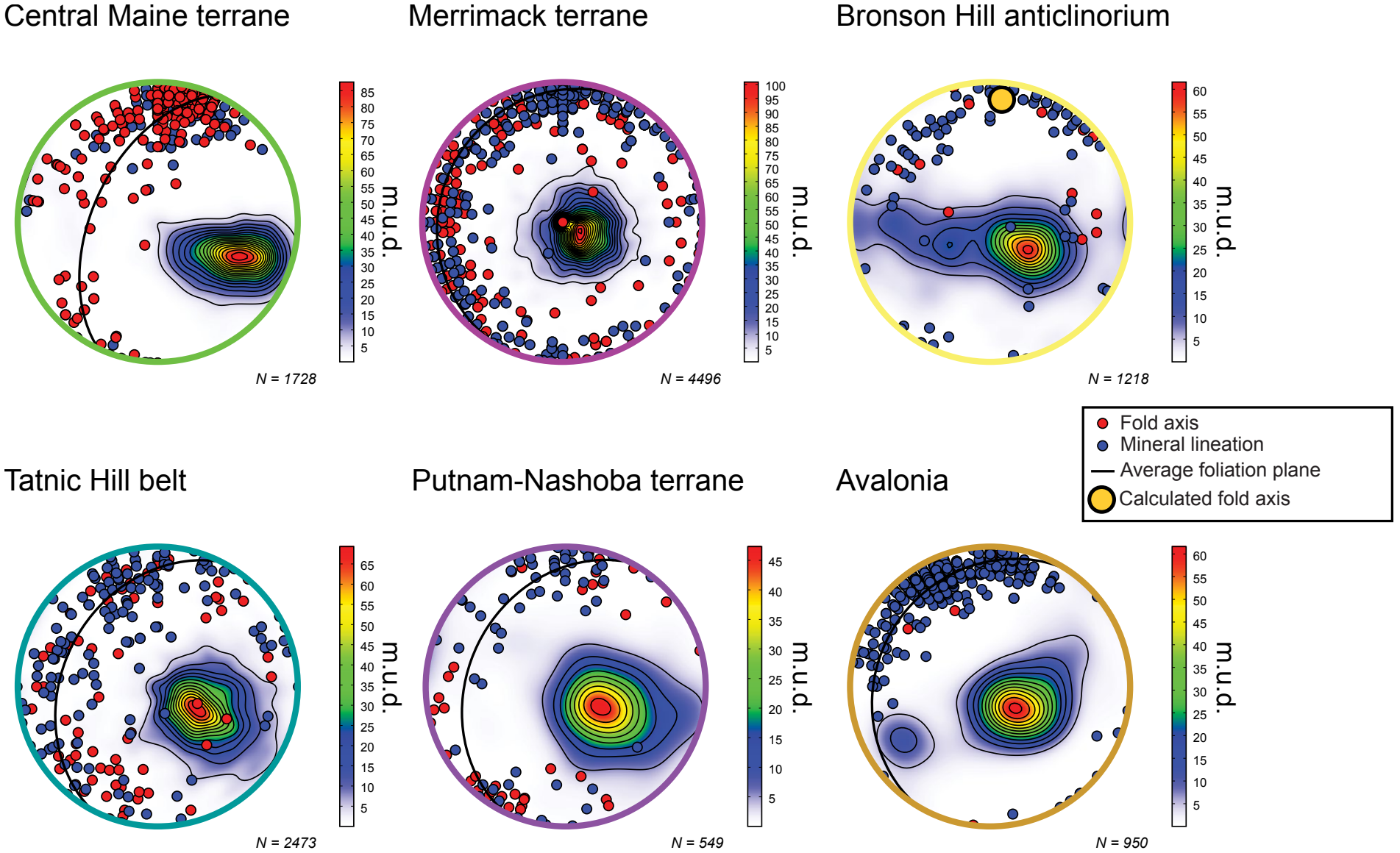

Figure 3. Stereonets of the compiled foliations (contoured by multiples of uniform density [m.u.d.]), mineral lineations (blue poles), and fold axes (red poles) separated by the tectonic domains on Figure 2. Average foliation plane is shown as a black arc, except for Bronson Hill anticlinorium. Due to large-scale folding within Bronson Hill anticlinorium, we plot the calculated fold axis as a large gold circle. Plotting was performed with Orient software (Vollmer, 1995, 2024). Data shown in this figure represent the entire structural dataset and are not averaged.

Connecticut are crosscut by a series of Late Devonian to Carboniferous high-angle reverse faults (Fig. 2; Zen et al., 1983; Rodgers, 1985). These fault zones sole out on the Eastford shear zone at the southern terminus of the Central Maine terrane in Connecticut (Figs. 1 and 2). Outcrop observations on vertical, E-W-striking faces in proximity to these high-angle fault zones—including asymmetric feldspar sigmoids, asymmetric west-side-up folding, and low-angle shallowly W-dipping shear bands—suggest Late Devonian to Carboniferous top-to-the-SE reverse faulting (e.g., Fig. 4A). Top-to-the-SE reverse faulting was likely contemporaneous with inferred shallow top-to-the-SE thrusting on the Eastford shear zone based on the regional map pattern (Fig. 2).

There is no documented dextral strike-slip shear zone on the eastern margin of the Central Maine terrane or Merrimack Terrane in southern New England correlating to the Norumbega shear zone to the north. In fact, many studies have documented a component of sinistral strike-slip deformation within and on the margins of the adjacent Putnam-Nashoba Terrane (Goldstein, 1989; Kruckenberg et al., 2019). We identified sinistral shear bands bounding late metamorphic quartz-rich boudins on subhorizontal outcrop faces in the eastern Central Maine terrane near Sturbridge, Massachusetts (e.g., Figs. 2 and 4B). Late Devonian dextral transpression was active to the east of the Bronson Hill anticlinorium and within the western Central Maine terrane and continued into the Early Carboniferous (Massey et al., 2017). While asymmetric shear sense indicators are identified on subhorizontal outcrop faces throughout the Bronson Hill anticlinorium and Central Maine terrane in southern New England, symmetric structures are abundant.

We analyzed microstructural shear sense indicators and quartz microstructures in two samples within the Central Maine terrane (CT2207 and MA2207; see Supplemental Text S3 for detailed petrographic and textural descriptions). Both samples are characterized by amoeboid grain boundaries and island grains (Fig. 5), indicative of high-temperature grain boundary migration in quartz. The plagioclase shape preferred orientation is strong in CT2207 but weak in MA2207. While both samples contain evidence for local simple shear, shear sense indicators in MA2207 do not conform to a single direction given that both sinistral and dextral sigmoids are present. The shear sense in CT2207 suggests a component of high-angle, top-to-the-E, reverse shear.

4.1.2 Monazite Textures and Geochemistry

In sample MA2207, we targeted four monazite grains for WDS compositional mapping (Figs. 6A–6D). The grains are subhedral to anhedral and are primarily localized within the biotite foliation. Based on monazite compositional and textural characteristics in the BSE images and WDS compositional maps (Fig. S15), we segregate monazite in this sample into four compositional domains: one core domain and three rim domains (Fig. 7).

Monazite trace element compositions for grains in sample MA2207 display a near-uniform negative slope from La to Lu on chondrite-normalized rare earth element (REE) diagrams with a weakly to moderately developed negative Eu anomaly (Fig. 7). Monazite REE trends are broadly correlated with the compositional zones delineated in Figure 7; however, there is partial overlap in the REE characteristics between zones. A Devonian monazite core, only present in grain 4, is characterized by relative depletion of Gd-Er in comparison to the rim domains (Fig. 7). The low- and moderate-Y rims of monazite are characterized by a negative Eu anomaly, whereas the high-Y rim (only measured on grain 4) lacks a Eu anomaly and is generally the most enriched monazite domain (Fig. 7).

Monazite in sample MA2207 yields concordant U-Pb dates spanning ca. 380–320 Ma (Figs. 8 and S1–S4). The cores yield a weighted mean age of 364 ± 5.2 Ma (mean square of weighted deviates [MSWD] = 0.63, N = 7). The inner, Y-rich rim yields a weighted mean age of 355 ± 1.4 Ma (MSWD = 1, N = 98). The inner, moderate-to-high-Y patchy rim (only visible in grain 3, Fig. 7) yields a weighted mean age of 345 ± 5 Ma (MSWD = 0.58, N = 7). The outermost, discontinuous high-Y rim (most visible on grains 1 and 4, Fig. 7) yields a weighted mean age of 340 ± 6 Ma (MSWD = 1.9, N = 5).

4.2 Eastford Shear Zone

4.2.1 Macro- and Microstructural Observations

In eastern Connecticut, the structural style transitions from moderately to steeply dipping fabrics within the Central Maine terrane to subhorizontal and shallowly dipping fabrics in the underlying Merrimack Terrane across the Eastford shear zone (Figs. 2 and 3). The Eastford shear zone is moderately W dipping along strike and to the north of its southernmost extent in Connecticut and may correlate, along strike, to Permo-Carboniferous strike-slip deformation on the subvertical Norumbega shear zone in southeastern Maine (e.g., Fig. 1). The Eastford shear zone crosscuts both the Central Maine terrane and Merrimack Terrane as a shallow N- to NW-dipping to subhorizontal décollement directly south of the Central Maine terrane. There is no macroscopic evidence of strike-slip or oblique simple shear along the Eastford shear zone based on the relative absence of asymmetric shear sense indicators on foliation-perpendicular and strike-parallel surfaces (i.e., subhorizontal planes). We document well-developed and pervasive top-to-the-SE shear sense indicators on the subvertical NW-SE-striking faces near the Eastford shear zone, supporting a component of top-to-the-SE thrusting (Fig. 4C).

We analyzed microstructural shear sense indicators and quartz microstructures in two samples within the Eastford shear zone (CT2205 and CT2208). Both samples contain evidence for high-temperature grain boundary migration and subgrain rotation recrystallization in quartz (island grains, subgrains, and pinning microstructures; see Fig. 5). Plagioclase in CT2205 forms sigmoidal aggregates with quartz that suggest a component of top-to-the-SE shear (clockwise rotation in section; Fig. 5). However, plagioclase in CT2208 displays no undulose extinction and no strong shape preferred orientation. The only evidence of asymmetry in sample CT2208 is the slight obliquity

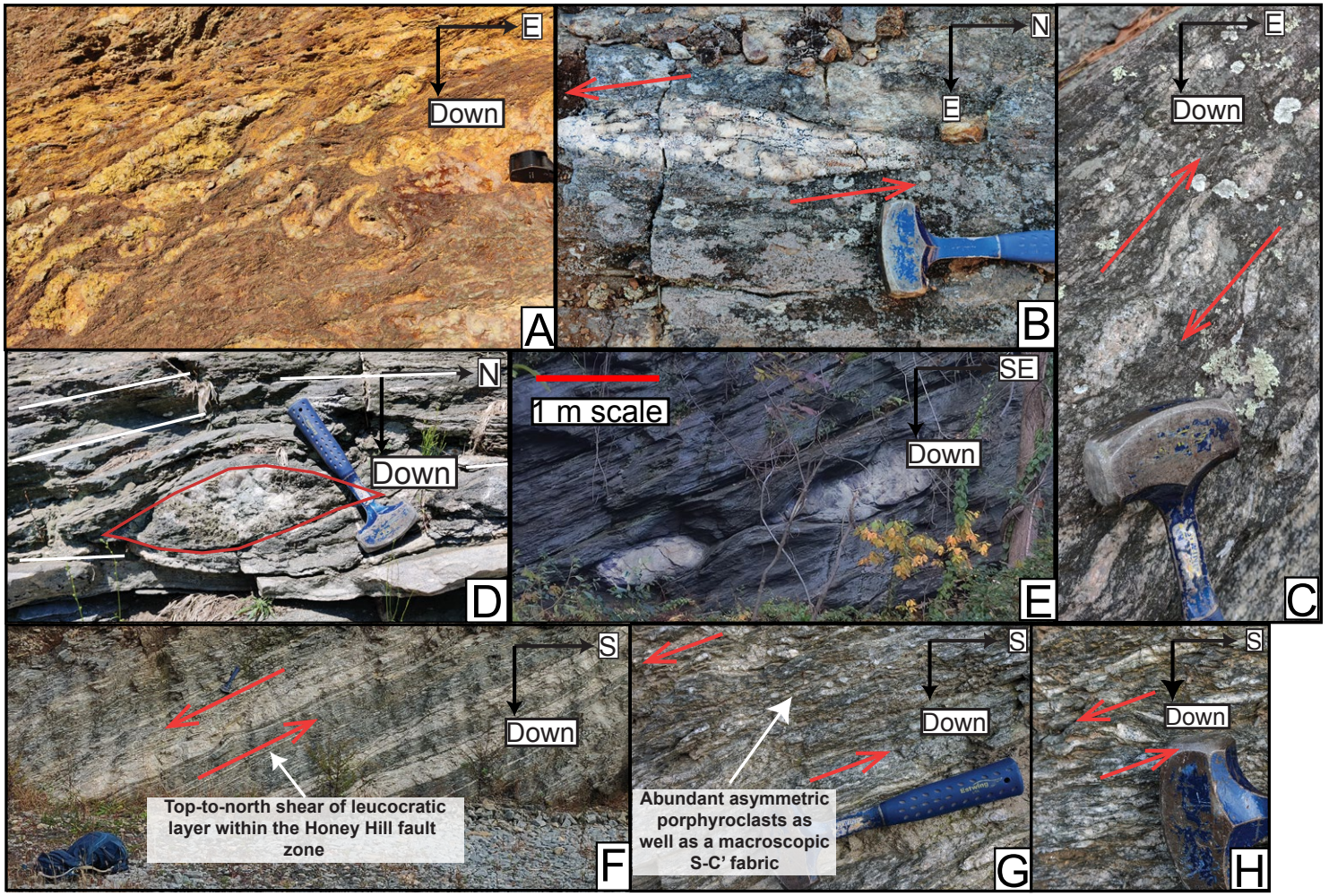

Figure 4. Outcrop photos of structures in southern New England (A—42°06′30.1″N 72°07′32.2″W; B—42°06′30.8″N 72°07′29.4″W; C—41°49′13.5″N 72°13′23.6″W; D—41°42′09.3″N 72°13′02.5″W; E—41°47′24.0″N 72°27′00.6″W; F—41°30′14.5″N 72°10′48.4″W; G—41°30′14.5″N 72°10′48.4″W; H—41°30′14.5″N 72°10′48.4″W). (A) Structures on subvertical exposure within Central Maine terrane near Sturbridge, Massachusetts, USA, displaying west-over-east asymmetric folding. Hand lens/loupe for scale (brand: Belomo). (B) Subhorizontal exposure at same locality as A, showing sinistral asymmetric boudin on subhorizontal plane. (C) Top-to-the-SE asymmetric shear band boudins within Eastford shear zone. (D) Boudin of coarse amphibole and plagioclase layer directly south of Willimantic, Connecticut, USA. Macroscopic foliation around boudin is delineated in white while boudin margins are delineated in red. There is a low-angle (<5°) top-to-the-N asymmetry of the boudin with respect to surrounding foliation. (E) Symmetric boudinage in core of Bolton synform in central Connecticut (F–H) Top-to-the-N shear sense indicators on outcrop through Honey Hill fault zone in southeastern Connecticut. In (F), 28 L Osprey backpack used for scale.

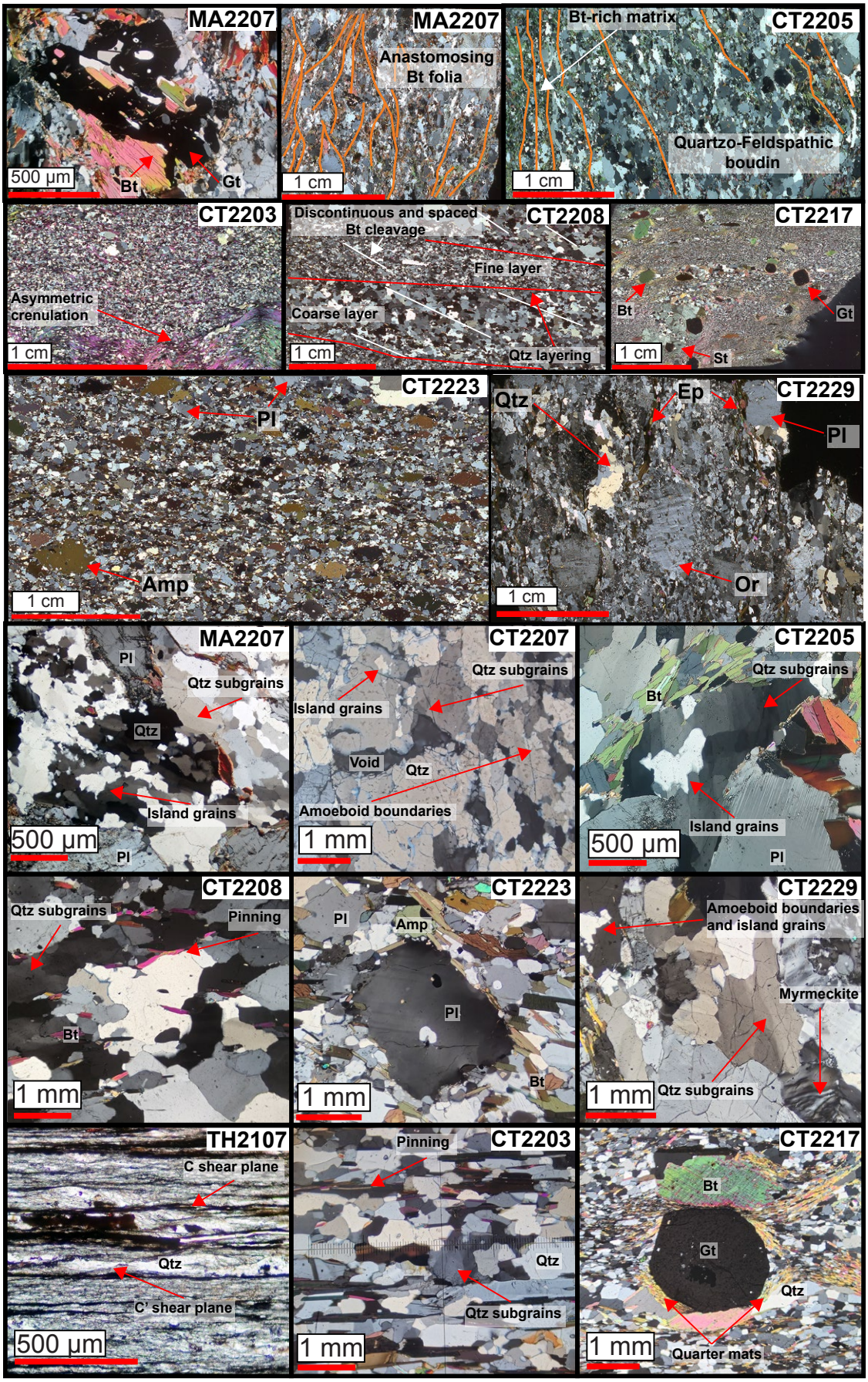

Figure 5. Select photomicrographs of sample textures. Thin-section-scale photomicrographs and a garnet texture from sample MA2207 are shown at top of figure. Sub-centimeter-scale features are shown in panels at base of figure. All panels are labeled by their sample number with notable structures and minerals discussed in text also labeled. All photomicrographs display textures in cross polarized light except for sample TH2107, which is shown in plane polarized light. See text and Supplemental Text S2 (see text footnote 1) for detailed discussion of textures in each sample. Bt—biotite; Gt—garnet; St—staurolite; Pl—plagioclase; Amp—amphibole; Ep—Epidote; Or—orthoclase; Qtz—Quartz.

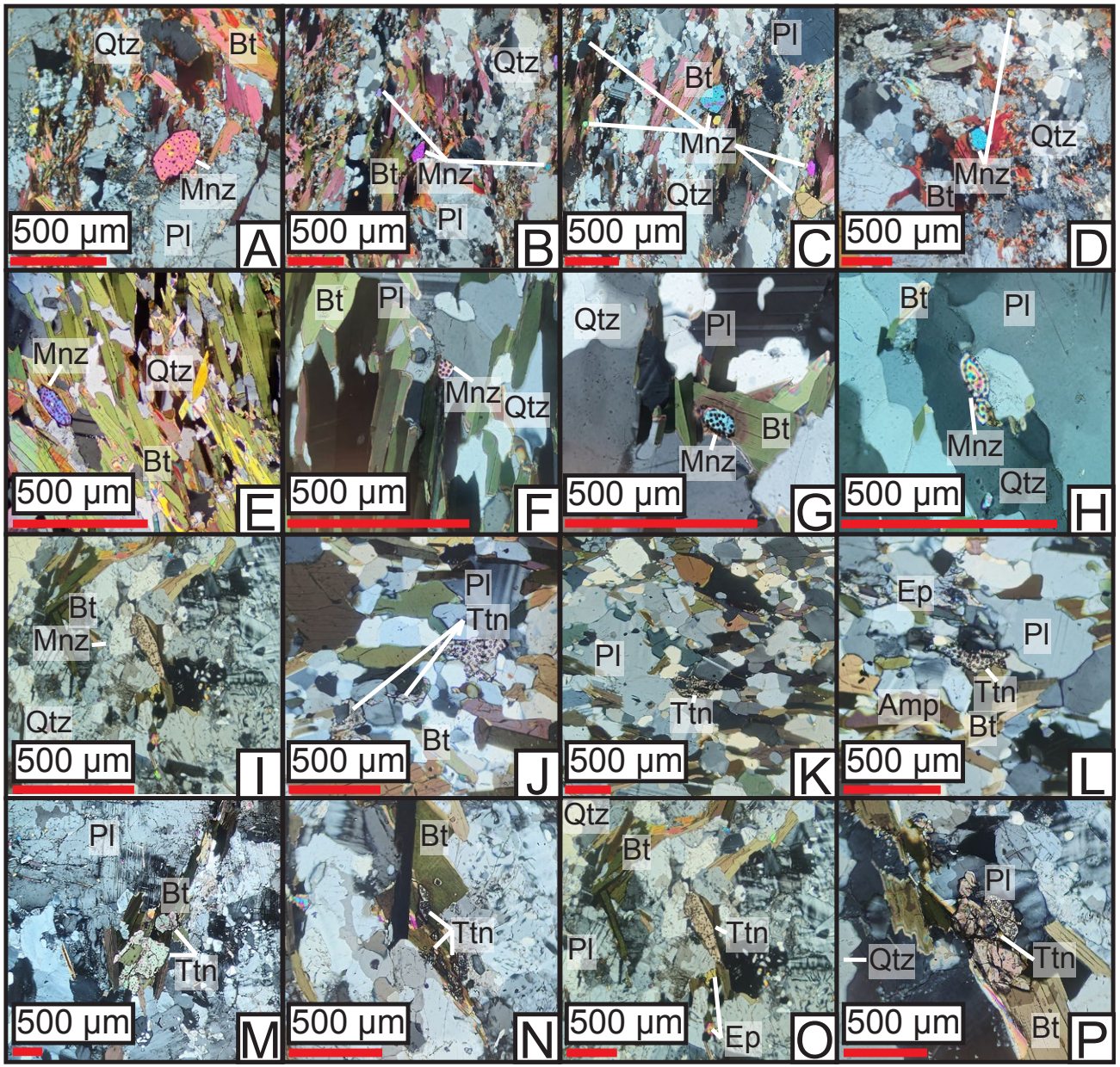

Figure 6. Monazite (A–I) and titanite (J–P) textures in cross polarized light from samples MA2207, CT2205, CT2223, and CT2229. See text for detailed description of textures. Major phases are labeled in white on each panel. A–D display monazite in sample MA2207. E–I display monazite in sample CT2205. J–L display titanite in sample CT2223. M–P display titanite in sample CT2229. Amp—amphibole; Bt—biotite; Ep—epidote; Mnz—monazite; Pl—plagioclase; Qtz—quartz; Ttn—titanite.

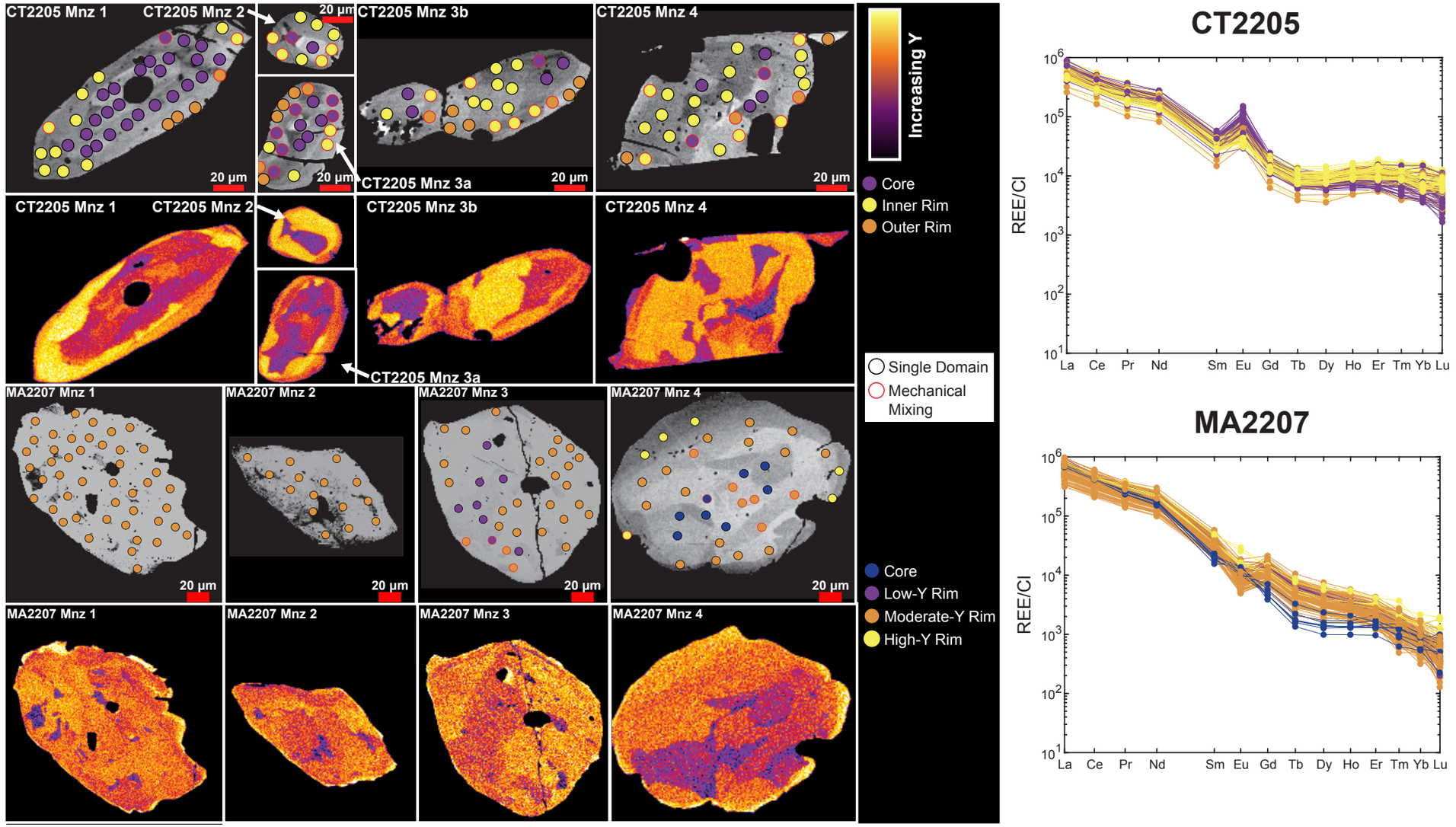

Figure 7. Monazite (Mnz) geochemistry and spot locations for samples CT2205 and MA2207. Backscattered electron maps overlain with spot locations colored by compositional zone are shown in addition to wavelength dispersive spectrometry compositional maps of Y in monazite. On right side of figure, chondrite-normalized (McDonough and Sun, 1995) rare earth element (REE) concentrations of each spot are shown. Each line on the REE plot represents an individual spot analysis with color indicating compositional zone. CI—Carbonaceous (Ivuna-type) chondrite.

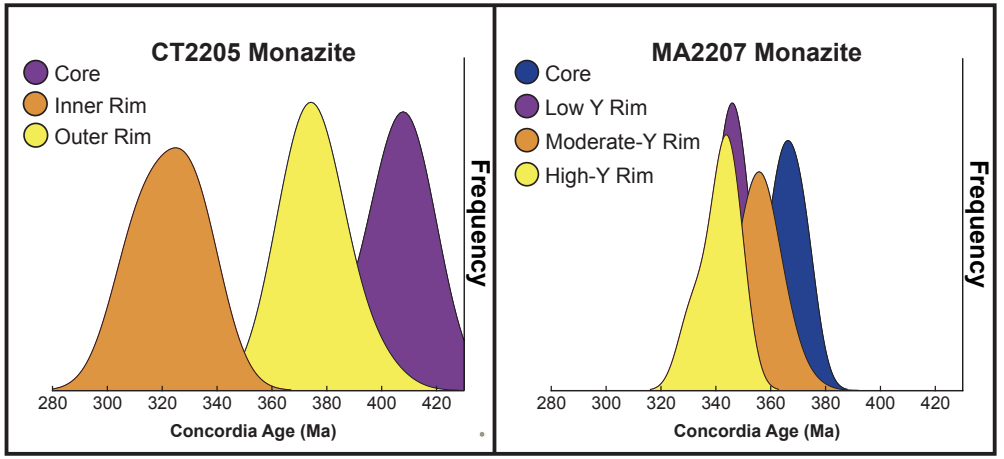

Figure 8. Kernel density estimates of monazite compositional zones in samples CT2205 and MA2207, with compositional zone colors corresponding to those in Figure 7. Ages were calculated for individual monazite spots based on U-Th-Pb equilibria in IsoplotR (Vermeesch, 2018). Weighted mean date for the compositional zone is calculated in IsoplotR, stated in text, and weighted mean diagrams are available in Figures S8–S14 (see text footnote 1).

(~10°–15°) of the discontinuous and spaced biotite foliation relative to a prominent, grain-size-dependent layering in quartz (Fig. 5). This obliquity between the mica cleavage and oblique quartz foliation would suggest a component of counterclockwise or top-to-the-E simple shear, but we note that this is a low-confidence interpretation.

4.2.2 Monazite Textures and Geochemistry

In sample CT2205, we targeted five individual grains of monazite for WDS compositional mapping and in situ LA-ICP-MS analysis (Figs. 6E–6I). The grains are subhedral to euhedral and are commonly elongated parallel to the quartz and biotite foliation (Figs. 6E–6I). Based on the observed compositional and textural characteristics in BSE and WDS imagery of the monazites, we identified three compositional domains (detailed analysis in Supplemental Text S3). These domains include a Y-poor core, a Y-rich inner rim, and a discontinuous moderate-Y-content outer rim (Fig. 7).

Monazite grains in sample CT2205 are characterized by steep light REE (LREE) slopes and shallow to horizontal slopes between Gd and Lu (Fig. 7). Additionally, sample CT2205 monazite displays strong positive Eu anomalies. Core domains have more negative heavy REE (HREE) slopes and a more positive Eu anomaly when compared to the rim domains (Fig. 7).

Monazite U-Pb dates in this sample range from ca. 430 Ma to 300 Ma (Fig. 8). The cores of monazite in this sample yield a weighted mean age of 405 ± 4 Ma (MSWD = 2, N = 38). The inner, Y-rich rim yields a weighted mean age of 375 ± 3 Ma (MSWD = 1.7, N = 35). The discontinuous outer rims, characterized by moderate Y contents, yield a weighted mean age of 324 ± 5 Ma (MSWD = 2, N = 14).

4.3 Merrimack Terrane

4.3.1 Macro- and Microstructural Observations

Outcrop observations on E-W- and N-S-striking planes within the Merrimack Terrane reflect largely coaxial strain or extremely high finite strains during noncoaxial deformation. Boudin geometries from the mantling gneiss in the core of Willimantic dome are weakly asymmetric within ~5°–10° of the macroscopic foliation (Figs. 2 and 4D)—that is, within reasonable uncertainty on the orientations of the foliation plane and boudin (~5°)—and may therefore reflect coaxial strain. Alternatively, the slight asymmetry may reflect a minor component of top-to-the-NW noncoaxial shear. Asymmetry in the surrounding Merrimack Terrane is present through a secondary cleavage plane, prominent in quartzo-feldspathic Devonian intrusions, which dips shallowly to moderately west. Lineations, boudin necks, and fold hinges vary significantly within the subhorizontal plane (Fig. 3). This may be a function of late, gentle to open folding about Willimantic dome, deforming an older set of lineations. Alternatively, a complex regional variation in lineation trends could reflect complex polyphase deformation. In general, most of the linear structures trend in the NE and SW quadrants (Fig. 3). These interpretations are consistent with late coaxial strains pervasive throughout the Merrimack Terrane, which deformed a pre-existing set of lineations in a coaxial manner. Our outcrop-scale observations suggest a component of high-strain top-to-the-NW deformation around Willimantic dome or, alternatively, coaxial strain, consistent with previous studies in the area (e.g., Getty and Gromet, 1992).

We analyzed microstructural shear sense indicators and quartz microstructures in two samples within the Merrimack Terrane (CT2223 and CT2229). Sample CT2223, located within the mantling Waterford Group gneiss around

Willimantic dome (Fig. 2), is characterized by an anastomosing, symmetric foliation defined by amphibole and plagioclase (Fig. 5). Sample CT2229 is from the Canterbury granite gneiss, which intruded the Merrimack Terrane in the Middle Devonian (414 ± 6 Ma U-Pb zircon crystallization age; Wintsch et al., 2007). CT2229 is characterized by an anastomosing, shallowly W-dipping foliation defined by plagioclase, orthoclase feldspar, and discontinuous biotite folia (Fig. 5). In contrast to the samples in the Central Maine terrane and Eastford shear zone discussed in sections 4.1 and 4.2, quartz is not significantly interconnected in these two samples.

CT2223 microstructures and nearby outcrop observations (Fig. 4D) suggest dominant coaxial (pure shear) deformation or high strain top-to-the-NW non-coaxial deformation. CT2229 microstructures may reflect either coaxial strain or dip-slip simple shear—it is not clear if there is a component of simple shear localized along the biotite basal planes in this case.

4.3.2 Titanite Textures, Electron Backscatter Diffraction (EBSD) Data, and Geochemistry

Titanite grains, elongate parallel to the foliation, were targeted in samples CT2223 and CT2229. As described in Supplemental Text S3, titanite grains in sample CT2223 are interstitial to the dominant amphibole, plagioclase, and quartz assemblage and align subparallel to the dominant foliation in the sample (Figs. 6J–6L). In sample CT2223, we analyzed three titanite grains (Figs. 6J–KL). All three grains are subhedral, and significant compositional zoning is absent in all three grains (Fig. S16).

In sample CT2229, we analyzed four titanite grains (Figs. 6M–6P). The four grains are subhedral to euhedral. Titanite grains in sample CT2229 are typically elongate parallel to subparallel with the biotite foliation (Figs. 6M–6P). While titanite is strongly localized in biotite folia in sample CT2229, there are no inclusions of biotite in titanite, suggesting titanite growth is syn- to post-metamorphic and kinematic with respect to the biotite foliation.

EBSD data for titanite in samples CT2223 and CT2229 are presented in Figure 9. In sample CT2223, the three grains display varying degrees of misorientation to the mean orientation of each grain ranging from 0° to 18°. Areas of significant misorientation are typically bound by subgrain boundaries; however, some areas characterized gradational and low-degree bending of the crystal lattice (<3°) do not result in subgrain development (i.e., titanite 2 in sample CT2223, Fig. 9). In sample CT2229, the maximum misorientation within grains varies from 7° to 12°. In general, the deformed areas are localized toward the rims of the crystal in the case of larger grains (i.e., grains 1 and 3, Fig. 9). As in sample CT2223, most deformed sectors of the grains in sample CT2229 result in subgrain development aside from sectors of diffuse and low-angle (<3°) misorientation.

The normalized REE element concentrations of titanite in sample CT2223 are relatively uniform (Fig. 10). This is consistent with the relatively homogeneous compositional zoning for titanite in this sample (Fig. S16).

The trace element compositional variation for titanites in sample CT2229 reflects the complex compositional zoning discussed in the Supplemental Material (Supplemental Text S3 and Figs. S16, 10, and 11). Within this sample, we identify three to four trace element zones on the basis of the observed variations in REE concentrations (Fig. 10). A REE-enriched titanite core domain is only observed in the core of grain 3. This zone is characterized by pronounced enrichment of the REEs and a negative Eu anomaly. A second zone, which we term the "inner rim", is observed in grains 1 and 3, composing the core of grain 1 and part of the rim of grain 3. This zone is characterized by an overall "flat" REE concentration profile with a positive Eu anomaly. In grain 3, this zone corresponds to very fine chemical zonations in Al and Nb (Fig. S16) and as a result of the fine character may include effects of mechanical mixing (i.e., domain mixing) with the young outer rim domain. We present data for the inner rim separately for grains 1 and 3 to isolate any mechanical mixing effects. Lastly, the "outer rim" titanite domains correspond to the rims of titanite grains 1 and 3 in this sample and also composes the entirety of grains 2 and 4. This zone is characterized by significant depletion of the LREEs relative to the HREEs and does not contain an observable Eu anomaly.

In sample CT2223, because there is very little compositional variation in the trace element concentrations, in the WDS maps of Al, Ce, Fe, and Nb, and in the U-Pb isotopic compositions (MSWD = 2.2), we report a single, inverse-isochron age of 269 ± 13 Ma (MSWD = 2, N = 144) for the three titanite grains in this sample (Fig. 11).

In sample CT2229, titanite dates span ca. 400–300 Ma (Figs. 11). The titanite core in grain 3 yields a U-Pb isochron age of 397 ± 11 Ma (MSWD = 1.5, N = 43). Titanite inner rims are separated between grains 1 and 3 to account for potentially significant mechanical mixing in grain 3 analyses. The inner rim in grain 1 yields an isochron age of 390 ± 8 Ma (MSWD = 6.4, N = 81). The inner rim in grain 3 yields an isochron age of 329 ± 26 Ma (MSWD = 4.2, N = 20). Titanite outer rims yield an isochron age of 307 ± 6 Ma (MSWD = 5.4, N = 123). The age of the inner rim zone in grain 3 overlaps with the outer rim age when considering the uncertainty on the isochron regressions. Such overlap could reflect mechanical mixing between the inner and outer rim domains in grain 3 spots. Interquartile ranges for titanite inner and outer rims are reported on Figure 11.

4.3.3 Zr-In-Titanite Thermometry

We calculated the temperature at which a given compositional domain in titanite (re)crystallized by utilizing the Zr concentrations following the method of Hayden et al. (2008). The pressure of titanite growth during Alleghanian metamorphism is the largest uncertainty in calculating titanite crystallization temperatures. Previous studies on Alleghanian metamorphism in eastern Connecticut suggest pressures of metamorphism of 0.7 ± 0.3 GPa (Moecher and Wintsch, 1994; Moecher, 1999; Wintsch et al., 2003). We ascribe a relatively large uncertainty to these pressure estimates due to the lack of sample coverage. Zr concentrations for the three titanite grains in sample CT2223

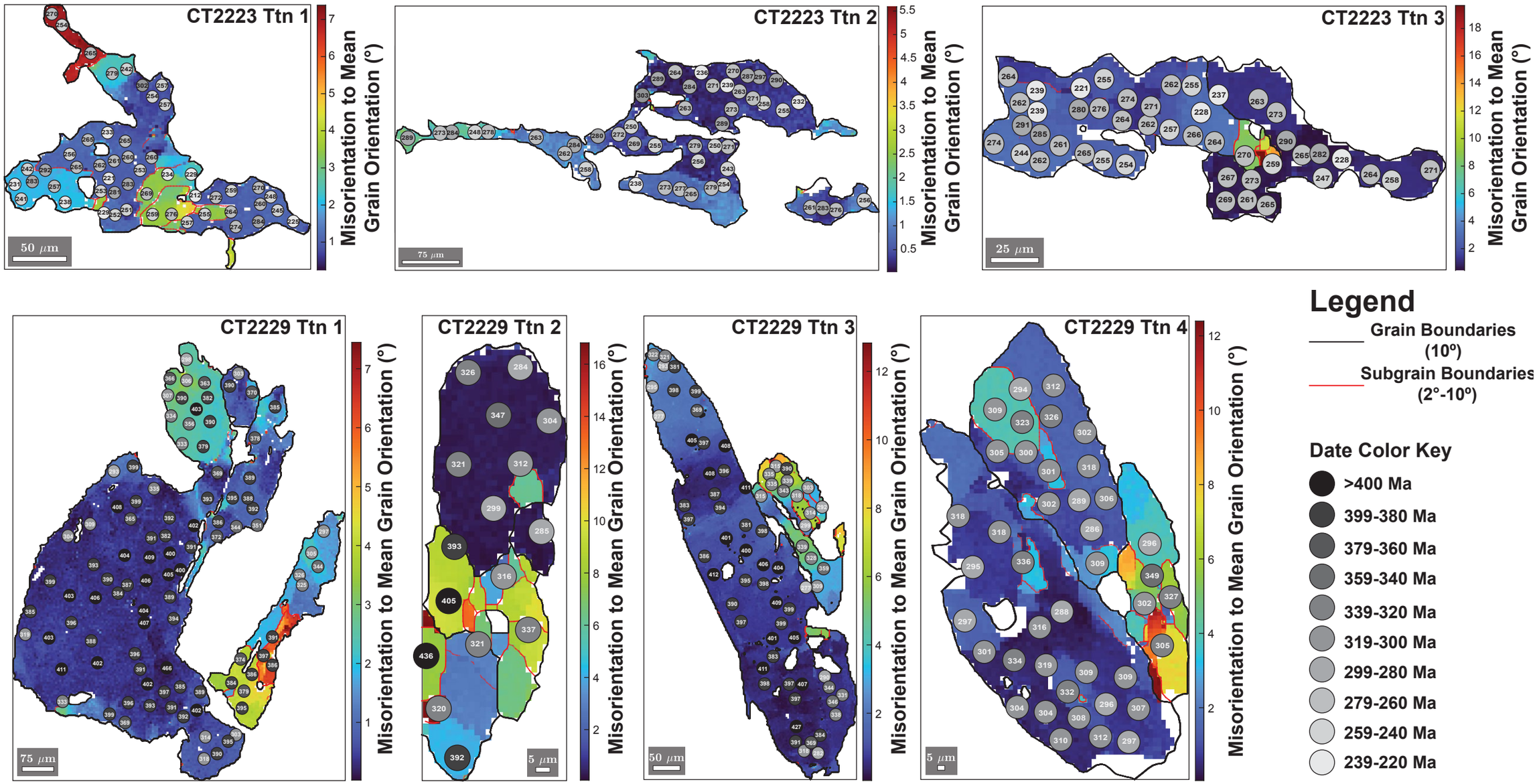

Figure 9. Titanite (Ttn) misorientation relative to mean grain orientation plots derived from electron backscatter diffraction analysis of titanites in this study. Plots were produced using MTEX toolbox (Bachmann et al., 2010). Degree values are grain boundary thresholds. Common-Pb-corrected spot ages are overlain to assess degree of U-Pb resetting in deformed versus undeformed parts of the crystal and colored in grayscale according to ages in the legend.

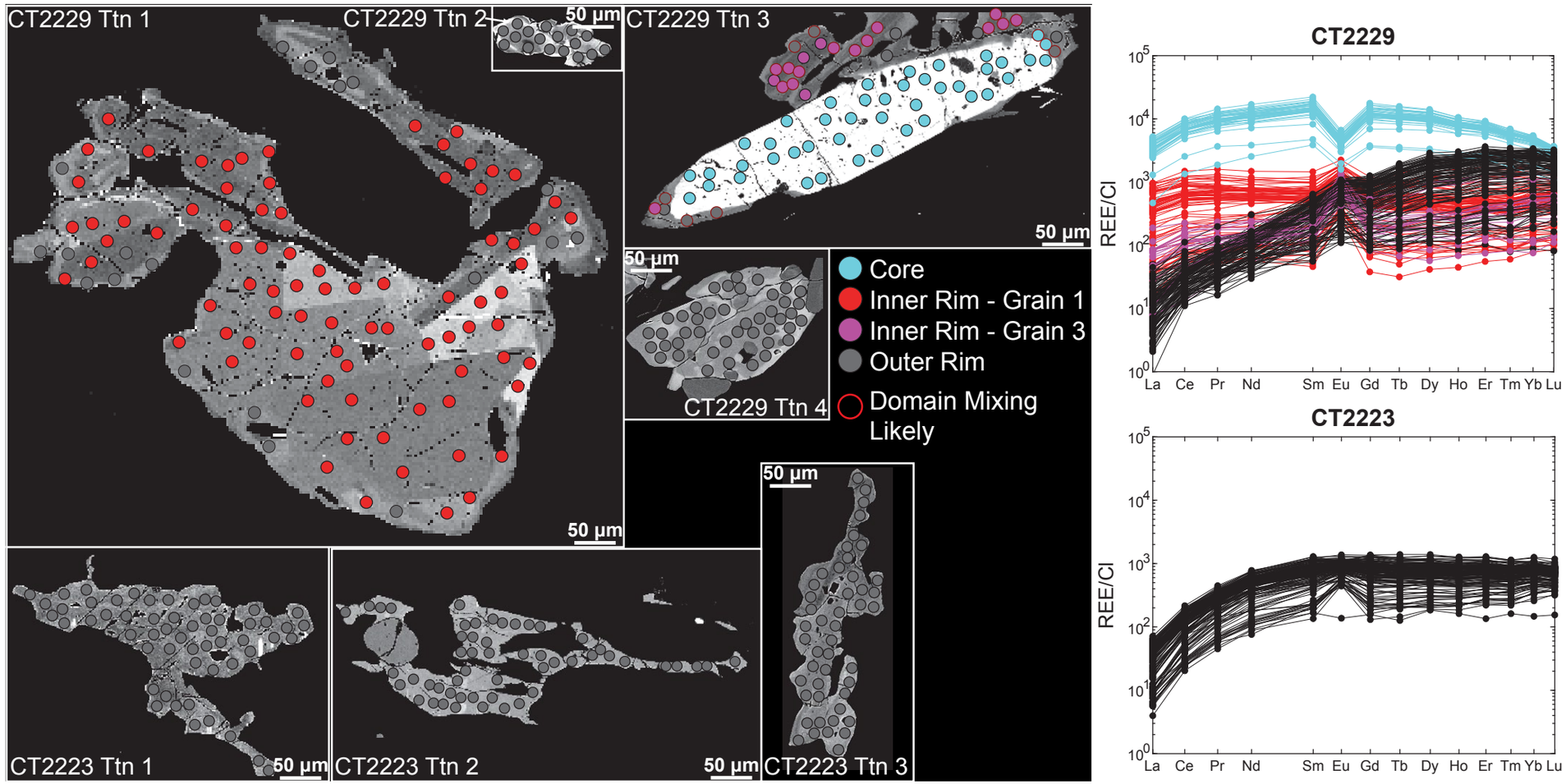

Figure 10. Titanite (Ttn) backscattered electron maps and spot locations as well as chondrite-normalized (McDonough and Sun, 1995) rare earth element (REE) diagrams for titanite grains in samples CT2229 and CT2223. Colors represent different trace element zones with distinct isotopic and trace element compositions. CI—Carbonaceous (Ivuna-type) chondrite.

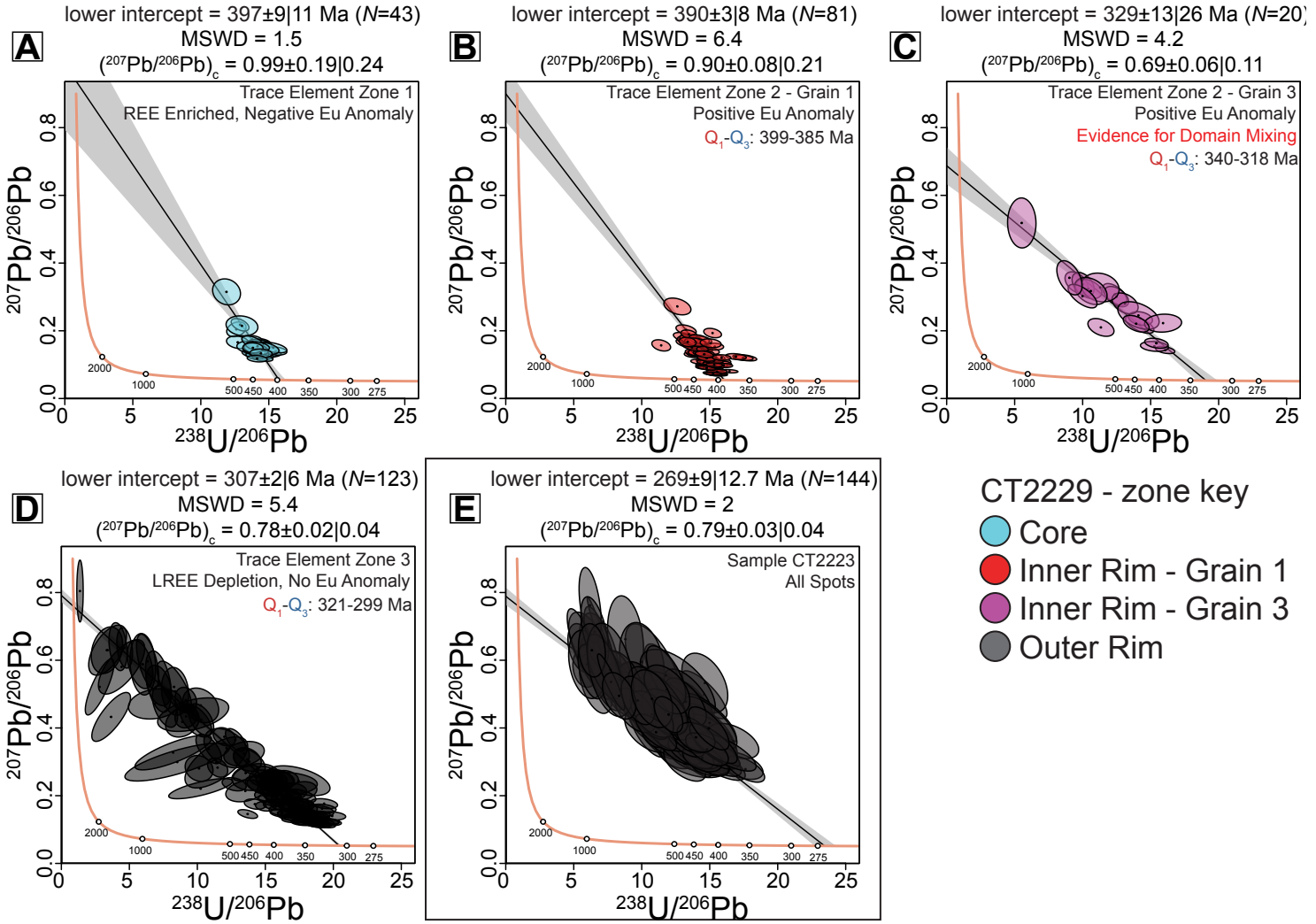

Figure 11. Tera-Wasserberg diagrams for U-Pb isotope compositions in four titanite grains from sample CT2229 and three titanite grains from sample CT2223 plotted in IsoplotR (Vermeesch, 2018). Panels A–D plot results of all spots for the three trace element zones in sample CT2229; colors of data points correspond to trace element domains identified in Figure 10. For each domain, we apply an unanchored isochron regression through the individual data, yielding two intercepts, a concordia intercept and a y-axis (common Pb [Pb_c]) intercept; the shading around the regression line is the 2s uncertainty of the regression through the data. The first error value is the 2s analytical uncertainty, the second value is the analytical uncertainty, accounting for overdispersion, by multiplying the 2s analytical uncertainty by the squareroot of the mean square of weighted deviates (MSWD). If MSWD of the isochron regression is >2, then we also present interquartile range (Q_1–Q_3) of common-Pb-corrected spot dates. Panel E shows data for sample CT2223 plotted together because they yield similar trace element compositions, U-Pb systematics, and relatively low MSWD (~2). REE—rare earth element; LREE—light REE.

yield temperatures of 630–725 °C, with the vast majority of temperatures lying between 640 °C and 700 °C (Fig. 12). Representative uncertainties on each temperature are ~37 °C based largely on the uncertainty in metamorphic pressure. Apart from four high-temperature spots out of a total of 483 spots (>700 °C), the titanite in this sample crystallized between ~630 °C and 700 °C.

Titanite in sample CT2229 displays a much larger range of Zr concentrations and associated (re)crystallization temperatures (Fig. 12). Zr concentrations in titanite for sample CT2229 range from ~15 ppm to 600 ppm, corresponding to temperatures from ~610 °C to 790 °C. The core in grain 3 yields the highest temperatures of 750–790 °C (Figs. 10 and 12). The Nb sector zones in grain 1 also record relatively high temperatures (Figs. 10 and 12, >700 °C). The rims of grains 1 and 3 and the entirety of grains 2 and 4 yield temperatures of ~620–700 °C (Fig. 12).

The distribution of titanite temperatures versus spot dates with associated uncertainties is shown in Figure 12. In general, we observe a wide range of titanite dates from as old as 460 Ma to as young as ca. 220 Ma. Additionally, we display a 2-D density plot of the individual data in Figure 12 and overlay the average Zr-in-titanite temperatures and isochron dates of each trace element domain.

From Figure 12, we note at least three episodes of titanite crystallization in the Merrimack Terrane. An Early to Middle Devonian episode of crystallization (trace element zones 1 and 2) is observed within the Canterbury Gneiss. A second and clearly distinct phase of titanite crystallization (titanite outer rims) occurred in the Carboniferous. Zr-in-titanite temperatures suggest that this episode took place at amphibolite facies conditions (>600 °C). In this case, despite the high MSWD, the isochron age is in broad agreement with the 2-D density plot. Lastly, we observe a latest Carboniferous to Permian phase of crystallization, only present in sample CT2223 from Willimantic dome. Titanite in sample CT2223 is geochemically reminiscent of titanite outer rims in sample CT2229. However, there is significantly less variation in concentrations of the medium REEs (MREEs) and HREEs in sample CT2223, resulting in a flatter slope across the entire profile (Fig. 10). The isochron age and temperature of titanite in sample CT2223 are generally inconsistent with previously published Ar-Ar geochronology for Willimantic dome. We discuss this inconsistency in section 5.2.

4.4 Bronson Hill Anticlinorium and Western Bronson Hill Shear Zone

The sinistral Western Bronson Hill shear zone extends from northeastern Vermont, along the Westminster West fault zone (Armstrong, 1997; McWilliams et al., 2013), to central Connecticut within the Bolton syncline (Massey and Moecher, 2013; Figs. 1 and 2). The Western Bronson Hill shear zone is steeply W-dipping to subvertical in northern New England. To the south, in central Connecticut, the shear zone is moderately to shallowly W-dipping (Fig. 2). The southern terminus of the Western Bronson Hill shear zone, and thus its maximum depth within the crust, is not well constrained. Previous work suggests that a sinistral shear system is present to the south of the Eastford shear zone and Bolton syncline in the Cremation Hill fault zone (London, 1988). However, there are no robust geochronologic constraints on the timing of this proposed deformation.

There is a clear shift in the orientation of foliations throughout the Bronson Hill anticlinorium beyond the southern terminus of the adjacent Central Maine terrane (Fig. 2, within the Bronson Hill anticlinorium and south of the locality 2, sample CT2217). Foliations are steeply to moderately dipping within the central Massachusetts and Vermont segments of the Western Bronson Hill shear zone. At latitudes south of the Eastford shear zone in Connecticut, the Western Bronson Hill shear zone rotates to moderate and shallow dips. Moreover, mineral stretching lineations within the Bolton syncline rotate toward a southerly dip direction. This suggests a transition in the overall deformation corresponding to either changing strain magnitude or a change in the deformation style (Fossen and Tikoff, 1998). Asymmetric kinematic indicators on both subvertical and subhorizontal outcrop surfaces become increasingly rare to the south, while symmetric boudins are abundant (e.g., Fig. 4E). The abundance of symmetric boudins, change in mineral lineation orientation, and rotation of the foliation all suggest that the sinistral strike-slip shear documented to the north wanes in central-eastern Connecticut in association with the disappearance of the Central Maine terrane across the Eastford shear zone.

We analyzed three thin sections along the Western Bronson Hill shear zone from central-eastern Vermont to south-central Connecticut (samples TH2107, CT2203, and CT2217; Fig. 2). The samples reflect both a north-to-south increase in metamorphic grade (muscovite to garnet and staurolite facies) as well as a north-to-south decrease in the component of sinistral simple shear (see Supplemental Text S2 for a detailed description of observations supporting this assertion).

4.5 Honey Hill–Lake Char Fault System

The Honey Hill–Lake Char fault system on the eastern and southern margins of the Merrimack Terrane likely records early Alleghanian underthrusting of Avalonia (Wintsch et al., 1992) followed by late Alleghanian (Permian) gravitational collapse and detachment faulting (Ma et al., 2023). The Honey Hill–Lake Char fault system has been relatively well characterized by a number of workers (e.g., Lundgren and Ebblin, 1972; Goldstein, 1989; Wintsch et al., 1992; Fleischer, 2022). Previous mapping efforts identified conflicting top-to-the-N and top-to-the-S shear sense along the Honey Hill fault zone and inferred that the top-to-the-S motion was most significant during the Carboniferous and Permian (Goldstein, 1989).

Our own outcrop observations suggest that top-to-the-N deformation was most significant during Late Carboniferous to Permian localized ductile deformation and exhumation. We observe well-developed and pervasive top-to-the-N asymmetric feldspar sigmoids and shear bands in a quartzo-feldspathic mylonite of the Honey Hill fault (Figs. 4F–4H). In contrast to the Merrimack

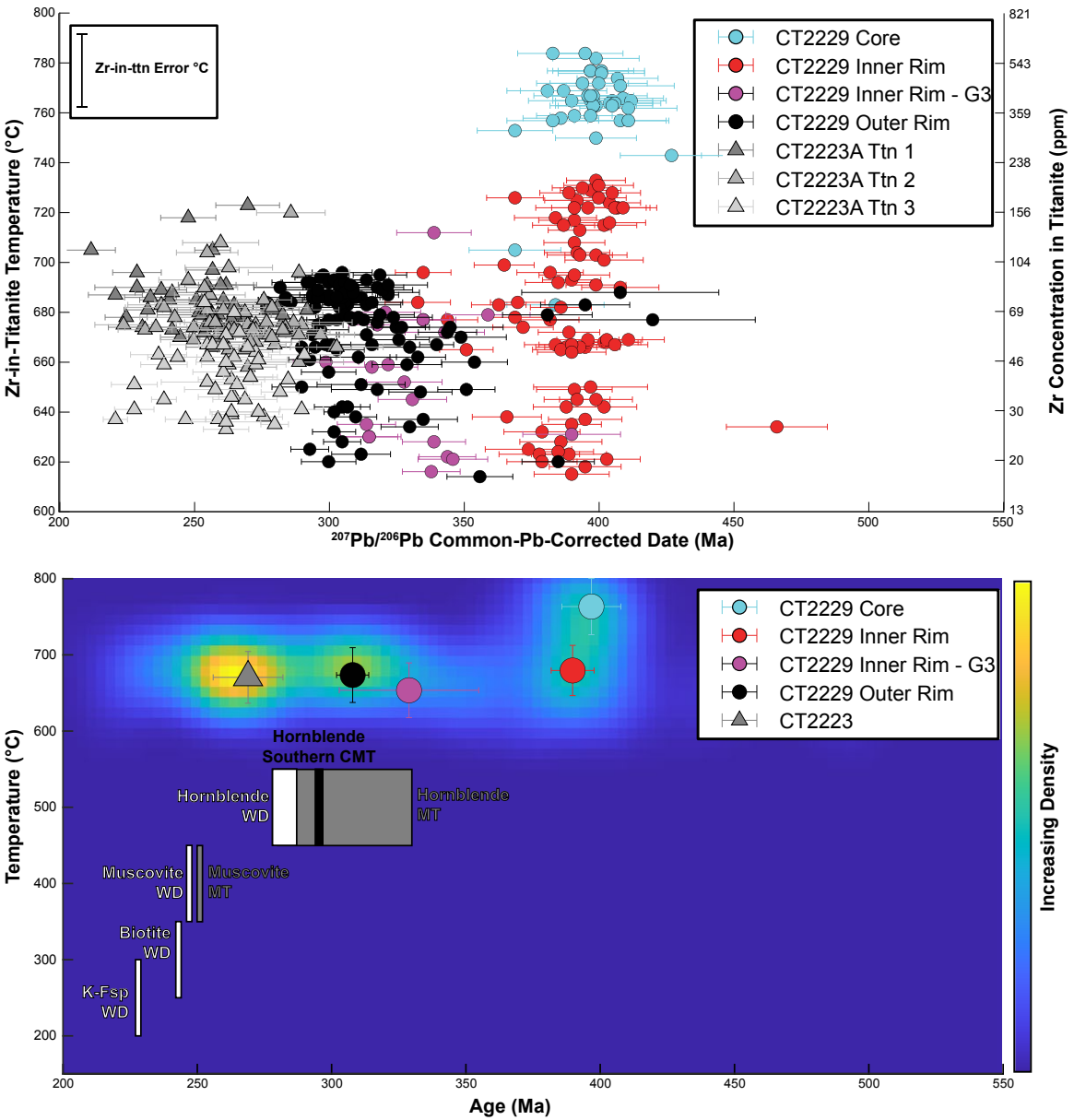

Figure 12. Top panel: Age of individual titanite spot analyses in samples CT2229 and CT2223, calculated as in Figure 11, plotted versus zirconium (Zr)-in-titanite temperature (corresponding Zr concentration is given on opposing *y*-axis) and colored by trace element zone. X-axis (age) error bars represent the 2s uncertainty of the date projected to concordia along the regression line. Zr-in-titanite uncertainty is essentially constant for each data point, based on a ±0.3 GPa pressure uncertainty and average pressure of 0.7 GPa, and is given in upper left corner. Bottom panel: Two-dimensional density plot of data shown in top panel, plotted with isochron ages and average temperatures of trace element zones in titanite and previously published Ar-Ar data from Wintsch et al. (1992, 1993). Errors on the bottom plot rectangles represent the range of dates from that method in the given region. Uncertainties on the titanite zone ages are from Figure 11. G3—grain 3; CMT—Central Maine terrane; MT—Merrimack Terrane; WD—Willimantic dome. Mineral abbreviations: K-Fsp—K-feldspar; Ttn—titanite.

Terrane, the metamorphism of Avalonia as exposed at the surface did not occur until the Late Carboniferous and early Permian (Wintsch et al., 1992).

5. DISCUSSION

5.1 Permo-Carboniferous Structure and Strain

5.1.1 Macro- and Microstructural Trends Within the Central Maine Terrane, Bronson Hill Anticlinorium, and Merrimack Terrane

The pattern of moderately to steeply W-dipping foliations and shallow to subhorizontal N-S-plunging mineral lineations and fold axes in the Central Maine terrane of central Massachusetts is traditionally interpreted as reflecting bulk dextral transpressional deformation during Acadian-Neoacadian orogenesis (Fossen and Tikoff, 1998; Massey et al., 2017; e.g., Figs. 2 and 3). Massey et al. (2017) interpreted the structure of central Massachusetts as reflecting dextral transpression during the Neoacadian orogeny from the Late Devonian into the Early Carboniferous.

Pervasive dextral simple shear is not observed in the eastern Central Maine terrane and Merrimack Terrane in central Massachusetts. Rather, we observed sinistral kinematic indicators on subhorizontal planes (e.g., Fig. 4B). Broadly, Silurian to Carboniferous sinistral kinematics are observed between the Putnam-Nashoba terrane and Avalonia within large late Paleozoic shear zone structures (e.g., Goldstein, 1989; Grimes and Skehan, 1995; Kruckenberg et al., 2019). Preliminary geochronologic analysis of the Putnam-Nashoba terrane suggests that sinistral motion occurred during the Middle Devonian and earliest Carboniferous (ca. 405–340 Ma; Buchanan et al., 2017; Severson, 2020). These results suggest that sinistral deformation in the eastern Central Maine terrane, Merrimack Terrane, and Putnam-Nashoba terrane is coeval with dextral transpression in the western Central Maine terrane. This implies south-directed lateral transport of the Central Maine terrane relative to adjacent terranes during the Late Devonian and Early Carboniferous.

Our analysis of the Permo-Carboniferous macrostructure and microstructure of southern New England suggests that localized, steep, strike-slip shear zones in the shallow crust (i.e., Norumbega shear zone and Western Bronson Hill shear zone, <15 km depth) transition to distributed coaxial strains and subhorizontal fabrics in the middle to lower crust beneath the Central Maine terrane (Figs. 1–3). Firstly, there is a clear macrostructural transition from steep regional fabrics to shallow regional fabrics across the Eastford shear zone in eastern Connecticut (Figs. 2 and 3). Additionally, we observe a transition in the lineation style across the Eastford shear zone. Mineral lineations and fold axes in the Central Maine terrane are mostly subhorizontal to shallowly north or south plunging (Fig. 3). In the Merrimack Terrane, mineral lineations and fold axes are all shallow to subhorizontal; however, they do not conform to a single trend (Fig. 3).

Traditional macrostructural relationships between the foliation and lineation in the Merrimack Terrane would suggest coaxial flattening or plane strains based on the relative absence of a preferred lineation direction. However, this assumes that the lineations all formed during a single deformation episode (i.e., Fossen et al., 1994). Therefore, while we cannot rule out a prior, Devonian or earliest Carboniferous phase of pervasive noncoaxial strain within the Merrimack Terrane (e.g., early, E-directed thrusting as implied by the stratigraphic relationships; Wintsch et al., 2007), the overall structural characteristics of the terrane suggest a final, pervasive episode of dominantly coaxial strain associated with localized top-to-the-NW simple shear.

Following from our previously mentioned observations regarding a transition from localized noncoaxial strike-slip strain to pervasive coaxial strains and localized top-to-the-NW extension in southern New England, we estimate a decreasing component of noncoaxial strain from north to south along the Western Bronson Hill shear zone. The changing style of deformation along the Bronson Hill anticlinorium can be visualized in terms of the type and abundance of asymmetric shear sense indicators. Our northernmost sample (TH2107) is characterized by asymmetric sinistral S-C-C′ microstructures and asymmetric quartz pressure shadows around ilmenite porphyroclasts (Fig. 5). Sample CT2203 from the Western Bronson Hill shear zone in north-central Connecticut is characterized by asymmetric mica cleavage on the subhorizontal plane; however, there are comparatively few indicators of asymmetry in sample CT2203 relative to sample TH2107. This suggests a component of sinistral simple shear with perhaps a greater pure shear component of deformation in comparison to sample TH2107. The sample from the southernmost Western Bronson Hill shear zone (CT2217) lacks consistent and clear asymmetric shear sense indicators. In fact, the presence of symmetric and conjugate quarter mats around porphyroblasts (Fig. 5) suggests a dominant component of coaxial strain. Altogether, these observations indicate a decreasing component of sinistral simple shear from north to south along the Western Bronson Hill shear zone, with the southernmost Western Bronson Hill shear zone and Merrimack Terrane recording primarily coaxial strain.

5.1.2 Along-Strike Continuity of Permo-Carboniferous Dextral Shear in New England

Of relevance to this study is the change in Permo-Carboniferous deformation style, or kinematics, from north to south in the New England Appalachians. The Norumbega shear zone is not clearly continuous along strike of the orogenic system (e.g., Goldstein and Hepburn, 1999; Kuiper, 2016). While an episode of Permo-Carboniferous dextral strike-slip strain is well established along the main segment of the Norumbega shear zone in southeastern Maine (West and Lux, 1993; West and Hubbard, 1997; Wang and Ludman, 2003; Johnson et al., 2009; Price et al., 2012, 2016), there is no evidence of continued dextral simple shear along orogenic strike of the Norumbega shear zone through southeastern New Hampshire and east-central Massachusetts. In fact, as established in section 5.1.1, sinistral strain is inferred for east-central Massachusetts on the margins of the Putnam-Nashoba terrane during the

Late Devonian to Early Carboniferous (Goldstein, 1989; Grimes and Skehan, 1995; Kruckenberg et al., 2019; this study, Fig. 4B). On the western margin of the Merrimack Terrane, within the Eastford shear zone, we observe evidence of primarily top-to-the-SE thrusting (Fig. 4C).

Altogether, the western margin of the Bronson Hill anticlinorium displays clear evidence for sinistral strain in the north (Vermont) transitioning to coaxial strain in the south (Connecticut). The Eastford shear zone, which is continuous with the dextral Norumbega shear zone along orogenic strike (Fig. 1), is characterized by middle Carboniferous top-to-the-SE thrusting (Figs. 4 and 13). This is contemporaneous with dextral strike-slip strain on the Norumbega shear zone (e.g., West and Lux, 1993). Thus, we must invoke a mechanism to explain contemporaneous and conflicting shear sense along the eastern margin of the Central Maine terrane bordering the Merrimack Terrane. We observe that the regional strike of this interface does rotate from NE-SW in SE Maine to nearly N-S in eastern Connecticut (Fig. 1). This coupled with a WNW to NNW maximum horizontal stress direction may explain the variance in shear sense along strike. This model predicts a relatively abrupt transition in kinematic sense from north-central Massachusetts to southeastern New Hampshire on the basis of a rotation in the regional orogenic trend.

5.2 Temperature and Timing of Permo-Carboniferous Deformation

To investigate the exact conditions of deformation and the absolute timing of the deformation discussed in section 5.1, we integrate quartz microstructures (Fig. 5; see detailed discussion in Supplemental Text S2), Zr-in-titanite thermometry (Fig. 12), EBSD analysis of titanite, and in situ U-Pb and trace element analysis of monazite and titanite (Figs. 7–12; see section 4). We supplement our new observations and data with existing geochronology and studies of deformation and metamorphism in southern New England.

5.2.1 Western Bronson Hill and Norumbega Shear Zones

Firstly, along the Bronson Hill anticlinorium, there is a general decrease in metamorphic grade along major ductile shear zones based on previously published work and our own observations (Wintsch et al., 1992; Fig. 5). Around the locality for sample TH2107 (Fig. 2), we observed micaceous schists and phyllites characteristic of greenschist facies metamorphism. In the Bolton syncline in central Massachusetts and north-central Connecticut, we observed biotite-garnet schists and blastomylonites. At the southern terminus of the Bolton syncline, we observed biotite-garnet-staurolite schists. Migmatites are described even farther south along the Bronson Hill anticlinorium (Wintsch et al., 2003). A recent study by Hillenbrand et al. (2023a) resolves Alleghanian metamorphism and deformation localized around Pelham dome in central Massachusetts (Fig. 1). They identified rapid initial burial of the core of Pelham dome from ca. 325 Ma to 300 Ma, followed by extension and cooling from ca. 300 Ma to 250 Ma.

In central Vermont, for sample TH2107, ultrafine grain sizes (<10 μm; Fig. 5) and quartz microstructures are consistent with low-temperature (and/or high stress) bulge recrystallization or cataclasis. These observations are indicative greenschist facies (300–400 °C) quartz deformation, assuming a typical orogenic strain rate of 10^{-12} s^{-1} (Stipp et al., 2002). The previously mentioned observations are comparable to those for the Norumbega shear zone in coastal Maine (e.g., Price et al., 2016) but with the opposite sense of shear. We do not have an explicit constraint on the pressure of deformation in this sample (TH2107). If we assume a typical continental geothermal gradient of ~25 °C/km, the depth of deformation at 300–400 °C was ~12–16 km (i.e., ~0.3–0.4 GPa). Given that orogenic geotherms can be much steeper than typical continental geotherms (e.g., Derry et al., 2009; Cross et al., 2015; Sutherland et al., 2017), these are likely maximum depth constraints. Published Ar-Ar ages of deformed phyllonites in southeastern Vermont, within the Western Bronson Hill shear

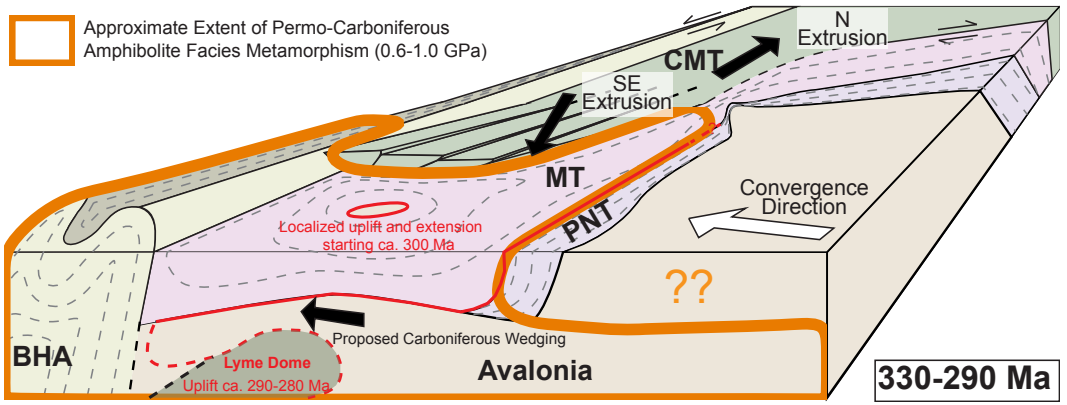

Figure 13. Schematic cross section of southern New England emphasizing Alleghanian structures and shear zones. Extrusion directions within Central Maine terrane (CMT) are indicated with black arrows. Approximate extent of Alleghanian amphibolite facies metamorphism (from Fig. 1) is overlain. Age of cooling and exhumation for Lyme dome is cited from Walsh et al. (2007). Proposed carboniferous wedging indicated is based on Wintsch et al. (2014). BHA—Bronson Hill anticlinorium; MT—Merrimack Terrane; PNT—Putnam-Nashoba Terrane.

zone, constrain the timing of low-temperature (~400 °C) deformation to ca. 300 Ma (McWilliams et al., 2013).

In central Massachusetts and north-central Connecticut, there is evidence for combined sinistral and compressive deformation (sinistral transpression) in the western Bronson Hill anticlinorium. Massey and Moecher (2013) identified an oblique sinistral, top-to-the-S shear zone on the western limb of the Bronson Hill anticlinorium. Massey et al. (2017) constrained the age of sinistral shear to ca. 330–290 Ma, consistent with Ar-Ar muscovite deformation ages for sinistral shear in Vermont (McWilliams et al., 2013). Sample CT2203 of this study is along strike of the locality studied by Massey and Moecher (2013). This sample is characterized by a sinistral asymmetric crenulation cleavage (Fig. 5). Sample CT2217 is south and along strike of sample CT2203 in central Connecticut. Microstructures in this sample suggest a significant component of coaxial strain based on symmetric mica quarter mats on garnet and biotite porphyroblasts (Fig. 5).

Altogether, we observe a transition from end-member sinistral strain in central Vermont to end-member coaxial strain in central Connecticut. Geochronologic constraints on the timing of this deformation span ca. 330–290 Ma based on monazite geochronology and Ar-Ar mineral ages in central Massachusetts (Massey et al., 2017) as well as Ar-Ar mica deformation ages in central Vermont (McWilliams et al., 2013).

5.2.2 Central Maine Terrane and Eastford Shear Zone

Previous studies found that most of the pervasive internal structure and metamorphism of the Central Maine terrane developed during Acadian-Neoacadian orogenesis between ca. 420 Ma and 340 Ma (Eusden and Barrerio, 1988; Massey et al., 2017; Moecher et al., 2021; Hillenbrand et al., 2023a). Ar-Ar amphibole plateau ages suggest that the Central Maine terrane in central Massachusetts and northern Connecticut, as well as the Putnam-Nashoba terrane, had cooled to <~500 °C by ca. 340–290 Ma (Spear and Harrison, 1989; Wintsch et al., 1992, 2003; Hillenbrand et al., 2021, 2023a; Ma et al., 2023). Ar-Ar white mica plateau ages suggest cooling to <~400 °C by ca. 300–250 Ma for much of the Central Maine terrane in New Hampshire and central Massachusetts (Harrison et al., 1989; Hillenbrand et al., 2021; Ma et al., 2023). Thus, the existing Ar-Ar data suggest that the Central Maine terrane was broadly at temperatures of 400–500 °C between 340 Ma and 250 Ma. Recent studies of metamorphic monazite crystallization and retrograde metamorphism in the Central Maine terrane of central Massachusetts have found that retrograde metamorphism, contemporaneous with regional transpression and lateral extrusion, began at ca. 350–340 Ma following Acadian-Neoacadian orogenesis (Hillenbrand et al., 2021, 2023a; Moecher et al., 2021).

In sample MA2207, from the Central Maine terrane in central Massachusetts, we find evidence of ductile plagioclase deformation based on undulose extinction in plagioclase grains (>600 °C; Tullis and Yund, 1992) and high-temperature quartz deformation (i.e., grain boundary migration and subgrain rotation recrystallization, >500 °C; Stipp et al., 2002; see also Fig. 5). Microstructures in this sample are indicative of bulk constriction and N-S lateral extrusion. A minimum age constraint on this high-temperature deformation is likely provided by old, late- to postkinematic monazite core domains (364 ± 5.2 Ma; Fig. 6).

We identify three monazite rim domains in sample MA2207 characterized by lobate-patchy textures or discontinuous outer rims. The Y-rich monazite rim domains are typically related to late-metamorphic, garnet-breakdown reactions and are therefore inferred to represent retrograde metamorphic crystallization of monazite throughout central Massachusetts (Massey et al., 2017; Hillenbrand and Williams, 2021; Hillenbrand et al., 2021, 2023a; Moecher et al., 2021). Thus, our findings of Y-rich monazite crystallization at 340 ± 6 Ma, 345 ± 5 Ma, and 355 ± 1 Ma are consistent with existing constraints on the timing of retrograde monazite crystallization in central Massachusetts.

Furthermore, the high to moderate Y contents and discontinuous lobate-cuspate rim textures (e.g., Fig. 7) indicate dissolution-reprecipitation recrystallization of monazite from ca. 355 Ma to 340 Ma. Dissolution-reprecipitation of monazite is commonly associated with fluid influx and may fully reset the U-Th-Pb dates of monazite at low-temperature (~450 °C) conditions (Williams et al., 2011). We posit that much of the retrograde monazite in this sample is recrystallized in the presence of a fluid, based on abundant lobate-cuspate, Y-rich rim growth around relict and resorbed Devonian monazite cores (e.g., Putnis, 2009; Williams et al., 2011). This fluid may have been generated by crystallization of Late Devonian granites observed throughout New England (e.g., Concord Granite: Lyons and Livingston, 1977; Harrison et al., 1987; Dorais, 2022; Hardwick Tonalite and Fitchburg Complex: Robinson et al., 1998), devolatilization reactions at depth (Stewart and Ague, 2018; e.g., from burial and heating of the Merrimack Terrane or other sedimentary protolith terranes beneath the Eastford shear zone), and/or channelization of an ambient fluid phase during localized ductile shearing and deformation (Connolly, 1997; Holcomb and Olsson, 2003).

Monazite grains in sample MA2207 are late to postkinematic based on their equant crystal shapes and crosscutting relationship with respect to the biotite foliation (Fig. 6). We interpret Carboniferous monazite rims in this sample to provide a minimum age constraint on deformation within the Central Maine terrane. Therefore, based on the available Ar-Ar cooling ages, our new monazite geochronology throughout the Central Maine terrane, quartz and plagioclase microstructures, and existing constraints on monazite crystallization from the literature (Massey et al., 2017; Hillenbrand et al., 2021, 2023a; Moecher et al., 2021), we conclude that there is little to no evidence of pervasive moderate- to high-temperature (>400 °C) deformation within the Central Maine terrane in central Massachusetts after ca. 340–330 Ma. This implies rigid to semi-rigid behavior of the Central Maine terrane in central Massachusetts and farther north in New Hampshire and Maine during the Late Carboniferous, with deformation localized onto general shear and dip-slip shear zones on the western and eastern margins of the Central Maine terrane, respectively, and localized high-angle reverse faults (e.g., Moecher et al., 2021). Moreover, these

data constrain the minimum age of paired dextral and sinistral transpressive strains on the margins of the Central Maine terrane.

Within the southernmost Central Maine terrane of northeastern Connecticut, near the Eastford shear zone, we observe relatively high-temperature (>500 °C) Permo-Carboniferous deformation and greenschist to amphibolite facies metamorphism overprinting prior Acadian-Neoacadian deformation and metamorphism. Samples CT2205, CT2207, and CT2208 all display high-temperature grain boundary migration (Fig. 5), which is typically associated with deformation temperatures >500 °C (Stipp et al., 2002; Toy et al., 2008). Deformed late-metamorphic assemblages in proximity to the Eastford shear zone typically contain quartz, plagioclase, biotite, white mica, and in some cases garnet.

Monazite in sample CT2205 is syn- to late kinematic with respect to the biotite foliation (Fig. 6). The cores of monazite grains in this sample yield a weighted mean age of 405 ± 4 Ma. The low-Y and high-Th characteristics of these cores could indicate crystallization during Early Devonian (Acadian) high-temperature metamorphism and partial melting (see Fig. S15 for compositional maps; Dumond et al., 2015). The Y-rich, inner rims of monazite in this sample are characterized by lobate-cuspate rim textures, whereas the moderate-Y outer rims are discontinuous around the grains (Fig. 7). As for sample MA2207, the high-Y characteristics and lobate-cuspate textures of the inner rims are likely indicative of monazite recrystallization during retrograde garnet breakdown and fluid-saturated conditions (dissolution-reprecipitation). However, the age of this breakdown (ca. 374 Ma; Fig. 8) is significantly older than suggested for central Massachusetts (ca. 350–340 Ma; Moecher et al., 2021; Hillenbrand et al., 2023a).

The early onset of retrograde metamorphism in our sample CT2205 may be indicative of the early metamorphic history of the Merrimack Terrane and disparate Devonian metamorphic conditions between the Central Maine terrane and Merrimack Terrane. The disparity in retrograde metamorphic timing compared with much of the monazite data in the Central Maine terrane (i.e., Massey et al., 2017, Moecher et al., 2021; Hillenbrand et al., 2023a) suggests that the protolith of sample CT2205 may belong to the Merrimack Terrane. Based on this assumption and the monazite data from this sample, the Merrimack Terrane did experience early metamorphism in the Devonian, followed by Late Devonian retrograde metamorphism at ca. 375 Ma.

The outermost discontinuous rim in sample CT2205 is the only Permo-Carboniferous monazite domain in this sample. This zone (ca. 324 Ma) is significantly younger than the monazite inner rims (ca. 375 Ma). Discontinuous rims argue for dissolution-reprecipitation. Moreover, the texture of the outer rim in grain 4 of this sample suggests there may have been dissolution-reprecipitation creep localized on opposing corners of the monazite grain. This texture is consistent with top-to-the-E simple shear and dissolution-reprecipitation creep monazite textures described by Dumond et al. (2022). Within the Central Maine terrane, such young monazite dates are only observed near major shear zones and faults (e.g., Moecher et al., 2021). Ar-Ar hornblende cooling dates in the southernmost Central Maine terrane suggest cooling below 500 °C by ca. 300–290 Ma (Fig. 12; Wintsch et al., 1995). Therefore, we interpret this monazite zone as reflecting fluid-reprecipitated monazite localized along shear zones during lower amphibolite (~500–550 °C) to upper greenschist (~450–500 °C) facies deformation.

Thus, top-to-the-SE deformation on the Eastford shear zone occurred during at least the middle to Late Carboniferous (ca. 330–300 Ma) but may have begun as early as the Late Devonian (ca. 375 Ma). At approximately the same time, the southernmost Central Maine terrane had cooled to temperatures of ~500 °C, and deformation was localized onto discrete high-angle reverse shear zones within the Central Maine terrane. Additionally, strike-slip shear occurred on discrete shear zones in the Western Bronson Hill (i.e., Massey and Moecher, 2013) and Norumbega shear zones. The interpretation of Carboniferous top-to-the-SE deformation on the Eastford shear zone implies Carboniferous loading of the underlying Merrimack Terrane, as suggested by some previous work (Fig. 1; Getty and Gromet, 1992; Wintsch et al., 1992, 2003, 2007). In conclusion, we suggest that the Merrimack Terrane may not have experienced the same high-grade metamorphic episode observed in the southern Central Maine terrane (i.e., Ague et al., 2013; Hillenbrand et al., 2023a). Consequently, the Merrimack Terrane did not experience post-Devonian metamorphism until Carboniferous loading in the footwall of the Eastford shear zone.

5.2.3 Merrimack Terrane and Willimantic Dome

We interpret the titanite grains in sample CT2223 to be synkinematic for several reasons. First, the titanite grains are parallel to the prominent plagioclase, amphibole, and biotite foliation (Fig. 6). Second, the titanite grains in this sample are characterized by relatively homogeneous compositions (Fig. 9) and yield a uniform population of U-Pb dates at ca. 269 ± 13 Ma (Fig. 11). This suggests a single episode of titanite crystallization rather than date complexities characteristic of resetting by dislocation creep and/or fluids (Moser et al., 2022, 2023). The grains are deformed and characterized by locally high misorientations (up to 18°) and subgrain development, displaying microstructures similar to those that have previously been interpreted to represent synkinematic titanite growth (Fig. 9; Moser et al., 2023). The U-Pb data as well as synkinematic textures (with respect to the primary amphibole + plagioclase + epidote assemblage; Fig. 5) and locally high EBSD misorientation angles suggest a single episode of metamorphic, synkinematic titanite crystallization at ca. 269 Ma.

The Zr-in-titanite temperatures from these titanite grains indicate the temperature of deformation was ~630–700 °C (Fig. 12). These data are inconsistent with Ar-Ar hornblende and mica plateau ages in the region, which indicate cooling to <~400–500 °C by ca. 280–260 Ma (Wintsch et al., 1992). This temperature discrepancy cannot be fully accounted for by the commonly cited Ar-Ar hornblende uncertainty of ±50 °C and potential uncertainties in Zr-in-titanite temperatures due to sector zoning (also ±50 °C; Walters and Kohn, 2017). An alternative explanation for this inconsistency may be extreme attenuation of

strata and a pre-existing thermal structure during exhumation and doming. Thus, our titanite U-Pb data, titanite microstructures, and average Zr-in-titanite temperatures support a phase of Permian amphibolite facies deformation proximal to Willimantic dome.

Titanite in sample CT2229 records a wide range of late Paleozoic dates, consistent with titanite (re)crystallization during Acadian and Alleghanian metamorphism. The titanite is localized within biotite-rich layers and generally parallel to the biotite foliation in the rock (Fig. 6). In contrast to titanite in sample CT2223, titanite in sample CT2229 displays pronounced compositional zoning (Fig. 10). We identified three trace element zones consistent with BSE textures (Fig. 10), compositional mapping (Fig. S16), and the trace element data.

Fe and Ce concentrations are relatively homogeneous in sample CT2229 titanites with the exception of grain 3, characterized by a euhedral core enriched in Fe and Ce and a subhedral to anhedral rim depleted in Fe and Ce. The core of grain 3 is characterized by an arcuate REE profile, with enrichment of the MREEs relative to the LREEs and HREEs, characteristic of magmatic titanite crystallization (Kohn, 2017). This titanite core yielded an average Zr-in-titanite temperature of 763 °C and an inverse isochron age of 397 Ma (MSWD = 1.5). The high Fe and Ce, REE concentrations, negative Eu anomaly, low EBSD misorientation angles (<2°), and high crystallization temperatures suggest that this core records igneous titanite crystallization at 397 Ma. The isochron age of this igneous titanite (397 ± 11 Ma) overlaps within the 2σ uncertainty of the igneous zircon crystallization age for the Canterbury Gneiss (414 ± 6 Ma; Wintsch et al., 2007).

Titanite inner rims are observed in two grains and characterized by a positive Eu anomaly and relatively "flat" variations in REE concentration (Fig. 10). We segregate the data in this trace element zone by grain because the spots in grain 3 were likely affected by significant mechanical mixing during LA-ICP-MS analysis. The isochron ages for titanite inner rims are significantly different between the two grains (Fig. 11). Grain 1 yields an inner rim isochron date of ca. 390 Ma, whereas grain 3 yields an inner rim isochron date of ca. 329 Ma. Both populations of inner rim data yield high MSWDs indicative of domain mixing, recrystallization, and/or prolonged crystallization. On inspection of inner rim spot placement and REE concentrations within grain 3, we observe that some spots overlap with the outer rim zone due to the fine diameter of the inner rim (<5 µm). Additionally, REE concentrations are much depleted in inner rim grain 3 spots as compared with the majority of inner rim grain 1 spots (Fig. 10). Both observations suggest that mechanical mixing between the inner and outer rim likely occurred for grain 3 spots and that inner rim spots from grain 1 are most characteristic of the age of this zone.

We interpret inner rim titanite (best constrained from grain 1) as reflecting Devonian high-temperature (~600–700 °C) metamorphism of the Merrimack Terrane during the Acadian orogeny. The MSWD of the inner rim titanite isochron (for both grains 1 and 3) is high (6.4 and 4.2 for grains 1 and 3, respectively). This indicates that inner rim titanite is not a simple product of single-stage (re)crystallization of titanite. The range of dates within titanite inner rims likely reflects partial to complete date resetting as a result of titanite deformation or fluid-related recrystallization (Gordon et al., 2021; Moser et al., 2022, 2023; Walters et al., 2022). EBSD misorientation data across inner rim domains are highly variable, with some portions characterized by extremely low (<1°) degrees of misorientation and other portions characterized by the highest degrees of misorientation in the crystal (up to 7°–12°; grains 1 and 3, Fig. 9). There is no clear correlation between dates in highly deformed domains compared to those in undeformed domains (Fig. 9), suggesting that inner rim dates do not solely reflect titanite deformation. This indicates that there is a decoupling of the trace element compositions (used to segregate the titanite domains) and U-Pb dates (Gordon et al., 2021; Moser et al., 2022; Walters et al., 2022). We propose that the second phase of titanite (re)crystallization corresponding to titanite inner rims is likely a product of partial to complete resetting of dates resulting from deformation and fluid-driven recrystallization. Thus, the youngest dates likely reflect a minimum deformation age.

Outer rim titanite in sample CT2229 yielded an isochron age of ca. 307 Ma (Figs. 11 and 12). As with the inner rim, the high MSWD of the inverse isochron (5.4; Fig. 11) indicates that these dates do not reflect a simple phase of titanite crystallization. The REE profiles of the outer rim data are characterized by depletion of the LREEs, no Eu anomaly, and a wide range of HREE enrichment (Fig. 10). The BSE and compositional zone textures of grains 2 and 4, which only yielded "inner rim" spots, display lobate-cuspate, Al-rich rims (Fig. S16). Lobate-cuspate rims suggest dissolution-reprecipitation of these titanite grains (e.g., Putnis, 2009; Moser et al., 2023). Furthermore, grains 2 and 4 are significantly deformed based on the EBSD data (Fig. 9). Given the Zr-in-titanite temperatures from the titanite outer rims (~610–690 °C), we propose that titanite outer rims (re)crystallized at amphibolite facies conditions, but this crystallization may reflect an admixture of (neo)crystallization, crystal-plastic deformation, and dissolution-reprecipitation in the presence of a fluid. Of these three processes, we see the most evidence for dissolution-reprecipitation based on lobate-cuspate textures within the grains (Fig. 10).

Titanite rims are characterized by a wide range of U-Pb dates, where those U-Pb dates do not display a clear correlation with trace element concentrations. Such decoupling may result from either crystal-plastic deformation (e.g., Gordon et al., 2021) or dissolution-reprecipitation in the presence of a fluid (e.g., Moser et al., 2022; Walters et al., 2022). Therefore, while titanite in sample CT2229 may have been synkinematic, the U-Pb dates no longer reflect synkinematic crystallization. The youngest dates likely bracket the minimum age of deformation to the Late Carboniferous (ca. 300–290 Ma; Fig. 12). Deformation significantly younger than this would likely have resulted in at least partial resetting of the U-Pb systematics.

Thus, Permo-Carboniferous titanite in sample CT2223 crystallized contemporaneous with to just preceding regional bulk coaxial strains and localized noncoaxial extensional strains between the Merrimack Terrane and underlying Avalonia. Crystallization within the Merrimack Terrane, best characterized by titanite in sample CT2229, suggests titanite (re)crystallization contemporaneous with top-to-the-SE deformation on the Eastford shear zone (Figs. 8, 11, and 12; ca. 330–300 Ma, this study). This suggests regional strain resulted from loading

of the overlying hanging wall and perhaps a component of prior top-to-the-SE and/or -E strain that is not well resolved in our sample. Crystallization around and within Willimantic dome, best characterized by sample CT2223, suggests titanite crystallization contemporaneous with exhumation and top-to-the-NW and/or -N extension on the Honey Hill–Lake Char fault system (Figs. 11 and 12; ca. 300–260 Ma; Wintsch et al., 1992; Fleischer, 2022). Furthermore, the significantly younger titanite dates observed in sample CT2223 as opposed to CT2229 suggest that titanite crystallization may have been progressively localized toward the mantle of Willimantic dome in the Permian during exhumation and cooling.

5.3 Implications for Permo-Carboniferous Orogenesis in Eastern North America

Our findings regarding Alleghanian metamorphism and deformation in southern New England imply a contrasting Alleghanian strain regime in the northern Appalachians relative to the southern Appalachians. Much of the existing work from the southern Appalachians suggests a dextral transpressive regime during the Permo-Carboniferous Alleghanian orogeny. Models of dextral strike slip combined with compression are primarily based on observations of the Brevard fault zone on the margins of the Piedmont Terrane (Gates et al., 1988; Secor et al., 1986; Hatcher, 2001). Some evidence from the southern Appalachians suggests a transition from strike-slip dominant deformation to shortening (dip-slip) dominant deformation in the middle Mississippian (ca. 350–330 Ma; Hibbard et al., 2010). In addition, Growdon et al. (2013) identified localized dextral simple shear in central-southern Connecticut, suggesting the transition to conjugate shear observed farther north in New England (coastal Maine) occurs in Connecticut to Massachusetts.

The character of Carboniferous deformation in New England, spanning ca. 350–300 Ma, is highly variable (Fig. 13). Hillenbrand et al. (2023a, 2023b) proposed that by ca. 350–340 Ma, the Central Maine terrane, Bronson Hill anticlinorium, and Waterbury dome experienced exhumation and retrograde metamorphism. They interpreted Pelham and Waterbury domes as forming during this stage of retrograde metamorphism. Ultimately, Hillenbrand et al. (2023a) concluded that the Carboniferous structure of central Massachusetts was produced during regional gravitational collapse and lateral extrusion, similar to some Himalayan gneiss domes (e.g., Hacker et al., 2017).

Contemporaneous with cooling and exhumation starting at ca. 350 Ma, the western Central Maine terrane experienced dextral transpression and the eastern Central Maine terrane experienced combined sinistral and top-to-the-E oblique simple shear (Massey et al., 2017; this study). Paired Carboniferous sinistral and dextral deformation on the margins of the Central Maine terrane suggests south-directed lateral extrusion during retrograde metamorphism (consistent with constriction in the center of the terrane, identified in sample MA2207 of this study; Fig. 5).

From ca. 330 Ma to 300 Ma, strike-slip strain was increasingly localized in discrete shear zones (Fig. 13). Dextral strain was localized within the Norumbega shear zone during ca. 300–290 Ma deformation. Sinistral strain was localized within the Western Bronson Hill shear zone at similar times (ca. 330–290 Ma; McWilliams et al., 2013; Massey and Moecher, 2013). Furthermore, localized Permo-Carboniferous dextral strain is observed within the Orange-Milford belt of central Connecticut (Growdon et al., 2013; Wintsch et al., 2024). Growdon et al. (2013) proposed that this belt, coupled with sinistral shear in the western Bronson Hill anticlinorium (McWilliams et al., 2013), likely resulted from the indentation of Gondwana about the New York Promontory.

Paired sinistral strike slip in the west and dextral strike slip in the east in northern New England (New Hampshire and Maine) implies north-directed lateral extrusion of the Central Maine terrane. In central Massachusetts and northeastern Connecticut, sinistral oblique transpression in the Western Bronson Hill shear zone was contemporaneous with top-to-the-SE thrusting and reverse faulting in the southeasternmost portion of the Central Maine terrane (Fig. 13). This implies combined regional compression and localized sinistral simple shear within the Western Bronson Hill shear zone in southern New England as well as bivergent north-south extrusion of the Central Maine terrane.

Contemporaneous with ca. 330–300 Ma north- and south-directed extrusion of the Central Maine terrane, the Merrimack Terrane experienced loading, and likely top-to-the-E simple shear in the footwall of the Eastford shear zone. This loading resulted in the pervasive, now shallow, planar fabric observed within the Merrimack Terrane. Although the fabric formed during the Carboniferous, we propose that the modern-day subhorizontal orientation, a characteristic of the entire Merrimack Terrane, is a product of near-symmetrical uplift of Willimantic dome.

Exhumation of Willimantic dome started at ca. 300 Ma and continued until at least ca. 260 Ma related to localized top-to-the- and/or -NW extension on the Honey Hill–Lake Char fault system and the related Willimantic fault. A pop-up of this top-to-the-N and/or -NW structure may also be exposed around Pelham dome in central Massachusetts, based on localized, young (Permian) cooling ages associated with the doming (Hillenbrand et al., 2023a).

We can reconcile the appearance of a sinistral shear zone in the northern as opposed to the southern Appalachians with two models for Alleghanian convergence in eastern North America: (1) zipper tectonics and lateral extrusion from the convergence between Laurasia and Gondwana (e.g., Vauchez et al., 1987; Hatcher, 2002; Growdon et al., 2013) or (2) gravitational collapse and northward extrusion of the upper crust in the northern Appalachians, driven by prior crustal thickening in the "Acadian altiplano" (e.g., Hillenbrand et al., 2021; Ma et al., 2023).

We propose a model for the Carboniferous based on zipper tectonics and lateral extrusion combined with gravitational collapse in an overall convergent plate boundary setting. Our proposed model invokes bivergent, lateral extrusion similar to the model of Growdon et al. (2013) but also integrates dextral shear on the Norumbega shear zone and east-directed thrusting on the Eastford shear zone. Our observations of top-to-the-E and/or -SE deformation in the Carboniferous require that the maximum stress was locally horizontal

in southern New England during Carboniferous deformation. Exhumation, cooling, and retrograde metamorphism of rocks in central Massachusetts during the Carboniferous may have resulted from exhumation and cooling of the hanging wall in a thrust fault or décollement as opposed to exhumation and cooling around an extensional detachment. In the northern Appalachians, we observe no significant Permo-Carboniferous thrusting. Rather, we propose north-directed extrusion of the Central Maine terrane between conjugate strike-slip shear zones (the Norumbega and Western Bronson Hill shear zones).

In southern New England (eastern Connecticut), extensional strain contemporaneous with regional exhumation clearly began by the latest Carboniferous to early Permian on the Honey Hill–Lake Char fault system (ca. 300–290 Ma; Figs. 11 and 12). This is consistent with observations of changing contractional to extensional deformation and associated amphibolite facies metamorphism within Avalonia (i.e., around Lyme dome at ca. 290–275 Ma; Walsh et al., 2007). This transition from Carboniferous thrusting to Permian extension demarcates the end of bivergent extrusion and late Paleozoic convergence in New England.

Models of purely gravitational collapse may satisfy observations of Carboniferous deformation in the northern New England Appalachians (e.g., Hillenbrand et al., 2023a) and Permian deformation in southern New England; however, a significant component of Carboniferous convergence and contraction is necessary to explain the structures and metamorphism in southern New England. Therefore, the Eastford shear zone and south-central Massachusetts may represent a fundamental transition point in southern New England, about which the primary driving mechanism of deformation in the orogenic belt transitions from gravitational collapse and north-directed extrusion in the northern New England Appalachians to south- and east-directed extrusion of the hanging wall coeval with thrusting and loading of the underlying Merrimack Terrane in the southern New England Appalachians.

Extrusion models have been previously proposed for the Alleghanian orogeny based on regional structural analysis in the Appalachians and Mauritinides (Africa; e.g., Vauchez et al., 1987; Hatcher, 2002; Growdon et al., 2013). Bivergent extrusion, as proposed herein, may have resulted from the collision of a Gondwanan promontory (i.e., the Reguibat promontory; Lefort, 1984) in the central Appalachians (Long Island Sound) or central Massachusetts. Bivergent extrusion may have also resulted from the convex geometry of the Gondwanan or Laurasian margin.

6. CONCLUSIONS

Carboniferous deformation in the northern New England Appalachians was characterized by steep, conjugate strike-slip shear zones in the shallow crust bounding a north-extruding semi-rigid to rigid Central Maine terrane. In central Massachusetts and northeastern Connecticut, the style of Carboniferous strain likely transitions from north-directed extrusion in the northern New England Appalachians to south-directed extrusion in the southern New England Appalachians. South-directed Carboniferous extrusion in southern New England (south-central Massachusetts and northeastern Connecticut) was coeval with top-to-the-E and/or -SE thrusting on the Eastford shear zone. This implies Carboniferous loading and prograde burial of the Merrimack Terrane. Carboniferous lateral extrusion was strongly overprinted in eastern Connecticut by top-to-the-N and/or -NW extension and associated coaxial flattening around Willimantic dome and the Honey Hill–Lake Char fault system. These constraints from southern New England suggest that gravitational forcing from high topography and high crustal thickness played a subsidiary role to northwest-southeast convergence in southern New England. However, at the same time, north-directed extrusion of the Central Maine terrane in New Hampshire and Maine may reflect near-end-member gravitational collapse, driven exclusively by gravitational potential of the Acadian altiplano. We propose a zipper extrusion model of Carboniferous tectonics in New England that reconciles observed south-directed extrusion in the southern Appalachians and southern New England with north-directed extrusion in northern New England. The flip from south- to north-directed extrusion was likely related to the plate boundary orientation of Gondwana and Laurasia or a localized northwest African promontory.

ACKNOWLEDGMENTS

We would like to acknowledge Ze Liu for assistance during the fieldwork associated with this manuscript; and Lauren Madsen and Piper Kramer for their assistance during LA-ICP-MS laboratory analysis at the University of Maine (Orono, Maine, USA). We also acknowledge Neel Chatterjee for his assistance in collecting EPMA maps at Massachusetts Institute of Technology (Cambridge, Massachusetts, USA). For fruitful discussions on the Alleghanian orogeny and New England Appalachian tectonics, we acknowledge Jay Ague and Maureen Long. We would like to thank Science Editor Christopher Spencer for the editorial handling of this manuscript as well as Associate Editor Mike Williams for his detailed insights and comments on the manuscript. We also thank Joshua Garber and one anonymous reviewer for their discerning reviews and comments on this extensive manuscript. This work was funded by the National Science Foundation under grant EAR-1925863.

REFERENCES CITED

Ague, J.J., Eckert, J.O., Chu, X., Baxter, E.F., and Chamberlain, C.P., 2013, Discovery of ultrahigh-temperature metamorphism in the Acadian orogen, Connecticut, USA: Geology, v. 41, p. 271–274, https://doi.org/10.1130/G33752.1.

Aiken, J.M., 1955, The bedrock geology of the Rockville quadrangle with map: Connecticut Geological and Natural History Survey Quadrangle Report 6, 55 p., 1 sheet, scale 1:31,680.

Aleinikoff, J.N., Wintsch, R.P., Fanning, C.M., and Dorais, M.J., 2002, U–Pb geochronology of zircon and polygenetic titanite from the Glastonbury Complex, Connecticut, USA: An integrated SEM, EMPA, TIMS, and SHRIMP study: Chemical Geology, v. 188, p. 125–147, https://doi.org/10.1016/S0009-2541(02)00076-1.

Aleinikoff, J.N., Wintsch, R.P., Tollo, R.P., Unruh, D.M., Fanning, C.M., and Schmitz, M.D., 2007, Ages and origins of rocks of the Killingworth dome, south-central Connecticut: Implications for the tectonic evolution of southern New England: American Journal of Science, v. 307, p. 63–118, https://doi.org/10.2475/01.2007.04.

Armstrong, T.R., 1997, Preliminary bedrock geologic map of the Vermont part of the 7.5 × 15 minute Bellows Falls quadrangle, Windham and Windsor Counties, Vermont: U.S. Geological Survey Open-File Report 97–284, scale 1:24,000, https://doi.org/10.3133/ofr97284.

Bachmann, F., Hielscher, R., and Schaeben, H., 2010, Texture analysis with MTEX—Free and open source software toolbox: Diffusion and Defect Data—Solid State Data: Part B, Solid State Phenomena, v. 160, p. 63–68, https://doi.org/10.4028/www.scientific.net/SSP.160.63.

Bird, J.M., and Dewey, J.F., 1970, Lithosphere plate-continental margin tectonics and the evolution of the Appalachian orogen: Geological Society of America Bulletin, v. 81, p. 1031–1060, https://doi.org/10.1130/0016-7606(1970)81[1031:LPMTAT]2.0.CO;2.

Blackburn, T.J., Olsen, P.E., Bowring, S.A., McLean, N.M., Kent, D.V., Puffer, J., McHone, G., Rasbury, E.T., and Et-Touhami, M., 2013, Zircon U-Pb geochronology links the end-Triassic extinction with the Central Atlantic Magmatic Province: Science, v. 340, p. 941–945, https://doi.org/10.1126/science.1234204.

Buchanan, J.W., II, Kuiper, Y.D., Hepburn, J.C., and Williams, M.L., 2017, Constraints on Devonian–Carboniferous deformation in the Nashoba terrane, eastern Massachusetts: Geological Society of America Abstracts with Programs, v. 49, no. 2, https://doi.org/10.1130/abs/2017NE-290834.

Chambers, J.A., and Kohn, M.J., 2012, Titanium in muscovite, biotite, and hornblende: Modeling, thermometry, and rutile activities of metapelites and amphibolites: American Mineralogist, v. 97, p. 543–555, https://doi.org/10.2138/am.2012.3890.

Chang, C.-P., Chang, T.-Y., Angelier, J., Kao, H., Lee, J.-C., and Yu, S.-B., 2003, Strain and stress field in Taiwan oblique convergent system: Constraints from GPS observation and tectonic data: Earth and Planetary Science Letters, v. 214, p. 115–127, https://doi.org/10.1016/S0012-821X(03)00360-1.

Collins, G.E., 1954, The bedrock geology of the Ellington quadrangle with map: Connecticut Geological and Natural History Survey Quadrangle Report 4, 44 p., 1 sheet, scale 1:31,680.

Connolly, J.A.D., 1997, Devolatilization-generated fluid pressure and deformation-propagated fluid flow during prograde regional metamorphism: Journal of Geophysical Research: Solid Earth, v. 102, p. 18,149–18,173, https://doi.org/10.1029/97JB00731.

Cross, A.J., Kidder, S., and Prior, D.J., 2015, Using microstructures and TitaniQ thermobarometry of quartz sheared around garnet porphyroclasts to evaluate microstructural evolution and constrain an Alpine Fault Zone geotherm: Journal of Structural Geology, v. 75, p. 17–31, https://doi.org/10.1016/j.jsg.2015.02.012.

Davies, J.H.F.L., Marzoli, A., Bertrand, H., Youbi, N., Ernesto, M., and Schaltegger, U., 2017, End-Triassic mass extinction started by intrusive CAMP activity: Nature Communications, v. 8, https://doi.org/10.1038/ncomms15596.

Dayem, K.E., Molnar, P., Clark, M.K., and Houseman, G.A., 2009, Far-field lithospheric deformation in Tibet during continental collision: Tectonics, v. 28, https://doi.org/10.1029/2008TC002344.

Deasy, R.T., and Wintsch, R.P., 2019, Draft bedrock geologic map of the Deep River quadrangle, New London and Middlesex Counties, Connecticut, USA: Connecticut Geological and Natural History Survey Open File 19-1, scale 1:24,000.

Derry, L.A., Evans, M.J., Darling, R., and France-Lanord, C., 2009, Hydrothermal heat flow near the Main Central Thrust, central Nepal Himalaya: Earth and Planetary Science Letters, v. 286, p. 101–109, https://doi.org/10.1016/j.epsl.2009.06.036.

Dixon, H.R., 1965, Bedrock geologic map of the Plainfield quadrangle, Windham and New London Counties, Connecticut: U.S. Geological Survey Geologic Quadrangle Map GQ-481, scale 1:24,000, https://doi.org/10.3133/gq481.

Dixon, H.R., 1968, Bedrock geologic map of the Danielson quadrangle, Windham County, Connecticut: U.S. Geological Survey Geologic Quadrangle Map GQ-696, scale 1:24,000, https://doi.org/10.3133/gq696.

Dixon, H.R., 1974, Bedrock geologic map of the Thompson quadrangle, Windham County, Connecticut, and Providence County, Rhode Island: U.S. Geological Survey Geologic Quadrangle Map GQ-1165, scale 1:24,000, https://doi.org/10.3133/gq1165.

Dixon, H.R., 1982, Bedrock geologic map of the Putnam quadrangle, Windham County, Connecticut: U.S. Geological Survey Geologic Quadrangle Map GQ-1562, scale 1:24,000, https://doi.org/10.3133/gq1562.

Dixon, H.R., and Felmlee, J.K., 1986, Bedrock geologic map of the Jewett City quadrangle, New London County, Connecticut: U.S. Geological Survey Geologic Quadrangle Map GQ-1575, scale 1:24,000, https://doi.org/10.3133/gq1575.

Dixon, H.R., and Pessl, F., 1966, Geologic map of the Hampton quadrangle, Windham County, Connecticut: U.S. Geological Survey Geologic Quadrangle Map GQ-468, scale 1:24,000, https://doi.org/10.3133/gq468.

Dixon, H.R., and Shaw, C.E., 1965, Geologic map of the Scotland quadrangle, Connecticut: U.S. Geological Survey Geologic Quadrangle Map GQ-392, scale 1:24,000, https://doi.org/10.3133/gq392.

Dorais, M.J., 2022, The petrogenesis and tectonic setting of the New Hampshire Plutonic Suite: Towards a more comprehensive model for the magmatism of the Acadian Orogeny: American Journal of Science, v. 322, p. 493–531, https://doi.org/10.2475/03.2022.03.

Dumond, G., Goncalves, P., Williams, M.L., and Jercinovic, M.J., 2015, Monazite as a monitor of melting, garnet growth and feldspar recrystallization in continental lower crust: Journal of Metamorphic Geology, v. 33, p. 735–762, https://doi.org/10.1111/jmg.12150.

Dumond, G., Mahan, K.H., Goncalves, P., Williams, M.L., and Jercinovic, M.J., 2022, Monazite as a monitor of shear strain in orogenic crust: Journal of Structural Geology, v. 161, https://doi.org/10.1016/j.jsg.2022.104672.

Eaton, G.P., and Rosenfeld, J.L., 1972, Preliminary bedrock geologic map of the Middle Haddam quadrangle, Middlesex County, Connecticut: U.S. Geological Survey Open-File Report 72-99, scale 1:24,000, https://doi.org/10.3133/ofr7299.

Eusden, J.D., Jr., and Barrerio, B., 1988, The timing of peak high-grade metamorphism in central-eastern New England: Maritime Sediments and Atlantic Geology, v. 24, p. 241–255, https://doi.org/10.4138/1654.

Eusden, J.D., Jr., and Lyons, J.B., 1993, The sequence of Acadian deformations in central New Hampshire, *in* Roy, D.C., and Skehan, J.W., eds., The Acadian Orogeny: Recent Studies in New England, Maritime Canada, and the Autochthonous Foreland: Geological Society of America Special Paper 275, p. 51–66, https://doi.org/10.1130/SPE275-p51.

Fahey, R.J., and Pease, M.H., 1977, Preliminary bedrock geologic map of the South Coventry quadrangle, Tolland County, Connecticut: Connecticut Geological and Natural History Survey Open File 94-584, scale 1:24,000.

Faure, S., Tremblay, A., and Angelier, J., 1996, Alleghanian paleostress reconstruction in the northern Appalachians: Intraplate deformation between Laurentia and Gondwana: Geological Society of America Bulletin, v. 108, p. 1467–1480, https://doi.org/10.1130/0016-7606(1996)108<1467:APRITN>2.3.CO;2.

Feininger, T., 1965, Bedrock geologic map of the Voluntown quadrangle, New London County, Connecticut, and Kent and Washington Counties, Rhode Island: U.S. Geological Survey Geologic Quadrangle Map GQ-436, scale 1:24,000, https://doi.org/10.3133/gq436.

Fetherston, D.B., Murray, D.P., and Wintsch, R.P., 2014, Alleghanian metamorphism of the southern Narragansett basin, RI: Hinged burial and exhumation, *in* Thompson, M.D., ed., Guidebook to Field Trips in Southeastern New England (MA-NH-RI): Wellesley, Massachusetts, USA, Wellesley College, p. B5-1–B5-20, https://digitalmaine.com/geo_docs/161.

Fleischer, N., 2022, Structural history of the Honey Hill fault and adjacent terranes in southeastern Connecticut, USA [M.S. thesis]: Golden, Colorado, USA, Colorado School of Mines, 110 p.

Fossen, H., and Tikoff, B., 1998, Extended models of transpression and transtension, and application to tectonic settings, *in* Holdsworth, R.E., Strachan, R.A., and Dewey, J.F., eds., Continental Transpressional and Transtensional Tectonics: Geological Society, London, Special Publication 135, p. 15–33, https://doi.org/10.1144/GSL.SP.1998.135.01.02.

Fossen, H., Tikoff, B., and Teyssier, C., 1994, Strain modeling of transpressional and transtensional deformation: Norsk Geologisk Tidsskrift, v. 74, p. 134–145.

Gates, A.E., Speer, J.A., and Pratt, T.L., 1988, The Alleghanian Southern Appalachian Piedmont: A transpressional model: Tectonics, v. 7, p. 1307–1324, https://doi.org/10.1029/TC007i006p01307.

Gerbi, C., and West, D.P., Jr., 2007, Use of U-Pb geochronology to identify successive, spatially overlapping tectonic episodes during Silurian-Devonian orogenesis in south-central Maine, USA: Geological Society of America Bulletin, v. 119, p. 1218–1231, https://doi.org/10.1130/B26162.1.

Getty, S.R., and Gromet, L.P., 1992, Evidence for extension at the Willimantic Dome, Connecticut: Implications for the late Paleozoic tectonic evolution of the New England Appalachians: American Journal of Science, v. 292, p. 398–420, https://doi.org/10.2475/ajs.292.6.398.

Ghent, E.D., and Stout, M.Z., 1984, TiO_2 activity in metamorphosed pelitic and basic rocks: Principles and applications to metamorphism in southeastern Canadian Cordillera: Contributions to Mineralogy and Petrology, v. 86, p. 248–255, https://doi.org/10.1007/BF00373670.

Goldsmith, R., 1967a, Bedrock geologic map of the Uncasville quadrangle, New London County, Connecticut: U.S. Geological Survey Geologic Quadrangle Map GQ-576, scale 1:24,000, https://doi.org/10.3133/gq576.

Goldsmith, R., 1967b, Bedrock geologic map of the Montville quadrangle, New London County, Connecticut: U.S. Geological Survey Geologic Quadrangle Map GQ-609, scale 1:24,000, https://doi.org/10.3133/gq609.

Goldstein, A.G., 1989, Tectonic significance of multiple motions on terrane-bounding faults in the northern Appalachians: Geological Society of America Bulletin, v. 101, p. 927–938, https://doi.org/10.1130/0016-7606(1989)101<0927:TSOMMO>2.3.CO;2.

Goldstein, A., and Hepburn, J.C., 1999, Possible correlations of the Norumbega fault system with faults in southeastern New England, *in* Ludman, A., and West, D.P., Jr., eds., Norumbega

Fault System of the Northern Appalachians: Geological Society of America Special Paper 331, p. 73–84, https://doi.org/10.1130/0-8137-2331-0.73.
Gordon, S.M., Kirkland, C.L., Reddy, S.M., Blatchford, H.J., Whitney, D.L., Teyssier, C., Evans, N.J., and McDonald, B.J., 2021, Deformation-enhanced recrystallization of titanite drives decoupling between U-Pb and trace elements: Earth and Planetary Science Letters, v. 560, https://doi.org/10.1016/j.epsl.2021.116810.
Grimes, S.W., and Skehan, J.W., 1995, Shear zones within the Bloody Bluff fault zone: Analysis and tectonic implications: Journal of Geodynamics, v. 19, p. 213–230, https://doi.org/10.1016/0264-3707(94)00015-N.
Growdon, M.L., Kunk, M.J., Wintsch, R.P., and Walsh, G.J., 2013, Telescoping metamorphic isograds: Evidence from $^{40}Ar/^{39}Ar$ dating in the Orange-Milford belt, southern Connecticut: American Journal of Science, v. 313, p. 1017–1053, https://doi.org/10.2475/10.2013.03.
Hacker, B.R., Ratschbacher, L., Rutte, D., Stearns, M.A., Malz, N., Stübner, K., Kylander-Clark, A.R.C., Pfänder, J.A., and Everson, A., 2017, Building the Pamir-Tibet Plateau—Crustal stacking, extensional collapse, and lateral extrusion in the Pamir: 3. Thermobarometry and petrochronology of deep Asian crust: Tectonics, v. 36, p. 1743–1766, https://doi.org/10.1002/2017TC004488.
Harrison, T.M., Aleinikoff, J.N., and Compston, W., 1987, Observations and controls on the occurrence of inherited zircon in Concord-type granitoids, New Hampshire: Geochimica et Cosmochimica Acta, v. 51, p. 2549–2558, https://doi.org/10.1016/0016-7037(87)90305-X.
Harrison, T.M., Spear, F.S., and Heizler, M.T., 1989, Geochronologic studies in central New England II: Post-Acadian hinged and differential uplift: Geology, v. 17, p. 185–189, https://doi.org/10.1130/0091-7613(1989)017<0185:GSICNE>2.3.CO;2.
Harwood, D.S., and Goldsmith, R., 1971, Bedrock geologic map of the Oneco quadrangle, Connecticut–Rhode Island: U.S. Geological Survey Geologic Quadrangle Map GQ-930, scale 1:24,000, https://doi.org/10.3133/gq930.
Hatcher, R.D., Jr., 2001, Rheological partitioning during multiple reactivation of the Palaeozoic Brevard Fault Zone, Southern Appalachians, USA, *in* Holdsworth, R.E., Strachan, R.A., Magloughlin, J.F., and Knipe, R.J., eds., The Nature and Tectonic Significance of Fault Zone Weakening: Geological Society, London, Special Publication 186, p. 257–271, https://doi.org/10.1144/GSL.SP.2001.186.01.15.
Hatcher, R.D., Jr., 2002, Alleghanian (Appalachian) orogeny, a product of zipper tectonics: Rotational transpressive continent-continent collision and closing of ancient oceans along irregular margins, *in* Martinez Catalán, J.R., Hatcher, R.D., Jr., Arenas, R., and Díaz García, F., eds., Variscan-Appalachian Dynamics: The Building of the Late Paleozoic Basement: Geological Society of America Special Paper 364, p. 199–208, https://doi.org/10.1130/0-8137-2364-7.199.
Hayden, L.A., Watson, E.B., and Wark, D.A., 2008, A thermobarometer for sphene (titanite): Contributions to Mineralogy and Petrology, v. 155, p. 529–540, https://doi.org/10.1007/s00410-007-0256-y.
Herz, N., 1955, The bedrock geology of the Glastonbury quadrangle with map: Connecticut Geological and Natural History Survey Quadrangle Report 5, 22 p., 1 sheet, scale 1:31,680.
Hibbard, J.P., van Staal, C.R., and Rankin, D.W., 2010, Comparative analysis of the geological evolution of the northern and southern Appalachian orogen: Late Ordovician-Permian, *in* Tollo, R.P., Bartholomew, M.J., Hibbard, J.P., and Karabinos, P.M., eds., From Rodinia to Pangea: The Lithotectonic Record of the Appalachian Region, Geological Society of America Memoir 206, p. 51–69, https://doi.org/10.1130/2010.1206(03).
Hillenbrand, I., Williams, M.L., Jercinovic, M.J., Heizler, M.T., and Tjapkes, D.J., 2023a, Petrochronologic constraints on Paleozoic tectonics in southern New England, *in* Whitmeyer, S.J., Williams, M.L., Kellett, D.A., and Tikoff, B., eds., Laurentia: Turning Points in the Evolution of a Continent: Geological Society of America Memoir 220, p. 505–532, https://doi.org/10.1130/2022.1220(25).
Hillenbrand, I.W., and Williams, M.L., 2021, Paleozoic evolution of crustal thickness and elevation in the northern Appalachian orogen, USA: Geology, v. 49, p. 946–951, https://doi.org/10.1130/G48705.1.
Hillenbrand, I.W., Williams, M.L., Li, C., and Gao, H., 2021, Rise and fall of the Acadian altiplano: Evidence for a Paleozoic orogenic plateau in New England: Earth and Planetary Science Letters, v. 560, https://doi.org/10.1016/j.epsl.2021.116797.
Hillenbrand, I.W., Williams, M.L., Peterman, E.M., Jercinovic, M.J., and Dietsch, C.W., 2023b, Petrochronologic constraints on inverted metamorphism, terrane accretion, thrust stacking, and ductile flow in the Gneiss Dome belt, northern Appalachian orogen: Journal of Metamorphic Geology, v. 41, p. 1197–1235, https://doi.org/10.1111/jmg.12741.
Holcomb, D.J., and Olsson, W.A., 2003, Compaction localization and fluid flow: Journal of Geophysical Research: Solid Earth, v. 108, https://doi.org/10.1029/2001JB000813.
Houari, M.-R., and Hoepffner, C., 2003, Late Carboniferous dextral wrench-dominated transpression along the North African craton margin (Eastern High-Atlas, Morocco): Journal of African Earth Sciences, v. 37, p. 11–24, https://doi.org/10.1016/S0899-5362(03)00085-X.
Johnson, S.E., Lenferink, H.J., Marsh, J.H., Price, N.A., Koons, P.O., and West, D.P., 2009, Kinematic vorticity analysis and evolving strength of mylonitic shear zones: New data and numerical results: Geology, v. 37, p. 1075–1078, https://doi.org/10.1130/G30227A.1.
Kapp, P., Manning, C.E., and Tropper, P., 2009, Phase-equilibrium constraints on titanite and rutile activities in mafic epidote amphibolites and geobarometry using titanite–rutile equilibria: Journal of Metamorphic Geology, v. 27, p. 509–521, https://doi.org/10.1111/j.1525-1314.2009.00836.x.
Karabinos, P., Macdonald, F.A., and Crowley, J.L., 2017, Bridging the gap between the foreland and hinterland I: Geochronology and plate tectonic geometry of Ordovician magmatism and terrane accretion on the Laurentian margin of New England: American Journal of Science, v. 317, p. 515–554, https://doi.org/10.2475/05.2017.01.
Kim, H.S., and Bell, T.H., 2005, Combining compositional zoning and foliation intersection axes (FIAs) in garnet to quantitatively determine early P-T-t paths in multiply deformed and metamorphosed schists: North central Massachusetts, USA: Contributions to Mineralogy and Petrology, v. 149, p. 141–163, https://doi.org/10.1007/s00410-004-0640-9.
Kinney, S.T., et al., 2022, Onset of long-lived silicic and alkaline magmatism in eastern North America preceded Central Atlantic Magmatic Province emplacement: Geology, v. 50, p. 1301–1305, https://doi.org/10.1130/G50181.1.
Kohn, M.J., 2017, Titanite petrochronology: Reviews in Mineralogy and Geochemistry, v. 83, p. 419–441, https://doi.org/10.2138/rmg.2017.83.13.
Kruckenberg, S.C., Michels, Z.D., and Parsons, M.M., 2019, From intracrystalline distortion to plate motion: Unifying structural, kinematic, and textural analysis in heterogeneous shear zones through crystallographic orientation-dispersion methods: Geosphere, v. 15, p. 357–381, https://doi.org/10.1130/GES01585.1.
Kuiper, Y.D., 2016, Development of the Norumbega fault system in mid-Paleozoic New England, USA: An integrated subducted oceanic ridge model: Geology, v. 44, p. 455–458, https://doi.org/10.1130/G37599.1.
Lefort, J.-P., 1984, Mise en evidence d'une virgation carbonifere induite par la dorsale Reguibat (Mauritanie) dans les Appalaches du Sud (U.S.A.): Arguments geophysiques: Bulletin de la Société Géologique de France, v. S7-XXVI, p. 1293–1303, https://doi.org/10.2113/gssgfbull.S7-XXVI.6.1293.
London, D., 1988, Characteristics and regional significance of the Cremation Hill ductile fault zone at the Bronson Hill-Merrimack boundary, south-central Connecticut: American Journal of Science, v. 288, p. 353–375, https://doi.org/10.2475/ajs.288.4.353.
Lundgren, L., Jr., 1979, The bedrock geology of the Haddam quadrangle with map: Connecticut Geological and Natural History Survey Quadrangle Report 37, 44 p., 1 sheet, scale 1:24,000.
Lundgren, L., Jr., and Ashmead, L.P., 1966, The bedrock geology of the Hamburg quadrangle with map: Connecticut Geological and Natural History Survey Quadrangle Report 19, 1 plate, scale 1:24,000, https://ngmdb.usgs.gov/ngm-bin/pdp/zui_viewer.pl?id=53519.
Lundgren, L., and Ebblin, C., 1972, Honey Hill fault in eastern Connecticut: Regional relations: Geological Society of America Bulletin, v. 83, p. 2773–2794, https://doi.org/10.1130/0016-7606(1972)83[2773:HHFIEC]2.0.CO;2.
Lundgren, L., Jr., Ashmead, L., and Snyder, G.L., 1971, The bedrock geology of the Moodus and Colchester quadrangles with maps: Connecticut Geological and Natural History Survey Quadrangle Report 27, 24 p., 2 sheets, scale 1:24,000.
Lyons, J.B., and Livingston, D.E., 1977, Rb-Sr age of the New Hampshire Plutonic Series: Geological Society of America Bulletin, v. 88, p. 1808–1812, https://doi.org/10.1130/0016-7606(1977)88<1808:RAOTNH>2.0.CO;2.
Ma, C., Hames, W.E., Foster, D.A., Xiao, W., Mueller, P.A., and Steltenpohl, M.G., 2023, Transformation of eastern North America from compression to extension in the Permian–Triassic, *in* Whitmeyer, S.J., Williams, M.L., Kellett, D.A., and Tikoff, B. eds., Laurentia: Turning Points in the Evolution of a Continent: Geological Society of America Memoir 220, p. 577–592, https://doi.org/10.1130/2022.1220(28).
Macdonald, F.A., Ryan-Davis, J., Coish, R.A., Crowley, J.L., and Karabinos, P., 2014, A newly identified Gondwanan terrane in the northern Appalachian Mountains: Implications for the Taconic orogeny and closure of the Iapetus Ocean: Geology, v. 42, p. 539–542, https://doi.org/10.1130/G35659.1.
Massey, M.A., and Moecher, D.P., 2013, Transpression, extrusion, partitioning, and lateral escape in the middle crust: Significance of structures, fabrics, and kinematics in the Bronson Hill

zone, southern New England, U.S.A.: Journal of Structural Geology, v. 55, p. 62–78, https://doi.org/10.1016/j.jsg.2013.07.014.
Massey, M.A., Moecher, D.P., Walker, T.B., O'Brien, T.M., and Rohrer, L.P., 2017, The role and extent of dextral transpression and lateral escape on the post-Acadian tectonic evolution of south-central New England: American Journal of Science, v. 317, p. 34–94, https://doi.org/10.2475/01.2017.02.
McDonough, W.F., and Sun, S.-s., 1995, The composition of the Earth: Chemical Geology, v. 120, p. 223–253, https://doi.org/10.1016/0009-2541(94)00140-4.
McWilliams, C.K., Kunk, M.J., Wintsch, R.P., and Bish, D.L., 2013, Determining ages of multiple muscovite-bearing foliations in phyllonites using the $^{40}Ar/^{39}Ar$ step heating method: Applications to the Alleghanian orogeny in central New England: American Journal of Science, v. 313, p. 996–1016, https://doi.org/10.2475/10.2013.02.
Moecher, D.P., 1999, The distribution, style, and intensity of Alleghanian metamorphism in south-central New England: Petrologic evidence from the Pelham and Willimantic Domes: The Journal of Geology, v. 107, p. 449–471, https://doi.org/10.1086/314359.
Moecher, D.P., and Wintsch, R.P., 1994, Deformation-induced reconstitution and local resetting of mineral equilibria in polymetamorphic gneisses: Tectonic and metamorphic implications: Journal of Metamorphic Geology, v. 12, p. 523–538, https://doi.org/10.1111/j.1525-1314.1994.tb00040.x.
Moecher, D.P., Cosca, M.A., and Hanson, G.N., 1997, Petrologic and $^{40}Ar/^{39}Ar$ geochronological constraints on the middle to late Paleozoic thermotectonic history of the southern Connecticut Valley zone, New England Appalachians: Geological Society of America Bulletin, v. 109, p. 164–175, https://doi.org/10.1130/0016-7606(1997)109<0164:PAAAGC>2.3.CO;2.
Moecher, D.P., McCulla, J.K., and Massey, M.A., 2021, Zircon and monazite geochronology in the Palmer zone of transpression, south-central New England, USA: Constraints on timing of deformation, high-grade metamorphism, and lithospheric foundering during late Paleozoic oblique collision in the Northern Appalachian orogen: Geological Society of America Bulletin, v. 133, p. 1021–1038, https://doi.org/10.1130/B35744.1.
Moore, G.E., 1983, Bedrock geologic map of the East Killingly quadrangle, Connecticut and Rhode Island: U.S. Geological Survey Geologic Quadrangle Map GQ-1571, scale 1:24,000, https://doi.org/10.3133/gq1571.
Moser, A.C., Hacker, B.R., Gehrels, G.E., Seward, G.G.E., Kylander-Clark, A.R.C., and Garber, J.M., 2022, Linking titanite U–Pb dates to coupled deformation and dissolution–reprecipitation: Contributions to Mineralogy and Petrology, v. 177, 42, https://doi.org/10.1007/s00410-022-01906-9.
Moser, A.C., Lusk, A.D., Attia, S., Garber, J.M., Seward, G.G.E., and Kylander-Clark, A.R.C., 2023, Titanite petrochronology records secular temperature and fluid evolution during ductile deformation: An example from Late Cretaceous shear zones in the Eastern Transverse Ranges: Geochemistry, Geophysics, Geosystems, v. 24, https://doi.org/10.1029/2022GC010855.
Murray, D.P., 1988, Post-Acadian metamorphism in the Appalachians, *in* Harris, A.L., and Fettes, D.J., eds., The Caledonian-Appalachian Orogen: Geological Society, London, Special Publication 38, p. 597–609, https://doi.org/10.1144/GSL.SP.1988.038.01.41.
O'Hara, K., 1986, Tectonic implications of late Paleozoic metamorphism in southeastern New England: Geology, v. 14, p. 430–432, https://doi.org/10.1130/0091-7613(1986)14<430:TIOLPM>2.0.CO;2.
Pease, M.H., 1972, Geologic map of the Eastford quadrangle, Windham and Tolland Counties, Connecticut: U.S. Geological Survey Geologic Quadrangle Map GQ-1023, scale 1:24,000, https://doi.org/10.3133/gq1023.
Pease, M.H., 1988, Bedrock geologic map of the Spring Hill quadrangle, Connecticut: U.S. Geological Survey Geologic Quadrangle Map GQ-1650, scale 1:24,000, https://doi.org/10.3133/gq1650.
Peper, J.D., and Pease, M.H., 1975, Geologic map of the Westford quadrangle, Connecticut: U.S. Geological Survey Geologic Quadrangle Map GQ-1214, scale 1:24,000, https://doi.org/10.3133/gq1214.
Price, N.A., Johnson, S.E., Gerbi, C.C., and West, D.P., 2012, Identifying deformed pseudotachylyte and its influence on the strength and evolution of a crustal shear zone at the base of the seismogenic zone: Tectonophysics, v. 518–521, p. 63–83, https://doi.org/10.1016/j.tecto.2011.11.011.
Price, N.A., Song, W.J., Johnson, S.E., Gerbi, C.C., Beane, R.J., and West, D.P., 2016, Recrystallization fabrics of sheared quartz veins with a strong pre-existing crystallographic preferred orientation from a seismogenic shear zone: Tectonophysics, v. 682, p. 214–236, https://doi.org/10.1016/j.tecto.2016.05.030.
Putnis, A., 2009, Mineral replacement reactions: Reviews in Mineralogy and Geochemistry, v. 70, p. 87–124, https://doi.org/10.2138/rmg.2009.70.3.
Rich, B.H., 2006, Permian bulk shortening in the Narragansett Basin of southeastern New England, USA: Journal of Structural Geology, v. 28, p. 682–694, https://doi.org/10.1016/j.jsg.2006.01.003.
Robinson, P., Tucker, R.D., Bradley, D., Berry, H.N., IV, and Osberg, P.H., 1998, Paleozoic orogens in New England, USA: GFF, v. 120, p. 119–148, https://doi.org/10.1080/11035899801202119.
Rodgers, J., 1985, Connecticut bedrock geology polygon: Hartford, Connecticut, Department of Environmental Protection, https://cteco.uconn.edu/metadata/dep/document/bedrock_geology_poly_fgdc_plus.htm (accessed November 2024).
Sacks, P.E., and Secor, D.T., Jr., 1990, Kinematics of late Paleozoic continental collision between Laurentia and Gondwana: Science, v. 250, p. 1702–1705, https://doi.org/10.1126/science.250.4988.1702.
Schlische, R.W., 1993, Anatomy and evolution of the Triassic-Jurassic Continental Rift System, eastern North America: Tectonics, v. 12, p. 1026–1042, https://doi.org/10.1029/93TC01062.
Secor, D.T., Snoke, A.W., and Dallmeyer, R.D., 1986, Character of the Alleghanian orogeny in the southern Appalachians: Part III. Regional tectonic relations: Geological Society of America Bulletin, v. 97, p. 1345–1353, https://doi.org/10.1130/0016-7606(1986)97<1345:COTAOI>2.0.CO;2.
Severson, A.R., 2020, Across- and along-strike structural and geochronological variations of the Nashoba-Putnam and Avalon terranes, eastern Massachusetts, Connecticut, and Rhode Island, southeastern New England Appalachians [Ph.D. thesis]: Golden, Colorado, USA, Colorado School of Mines, 131 p.
Sevigny, J.H., and Hanson, G.N., 1993, Orogenic evolution of the New England Appalachians of southwestern Connecticut: Geological Society of America Bulletin, v. 105, p. 1591–1605, https://doi.org/10.1130/0016-7606(1993)105<1591:OEOTNE>2.3.CO;2.
Snyder, G.L., 1961, Bedrock geology of the Norwich quadrangle, Connecticut: U.S. Geological Survey Geologic Quadrangle Map GQ-144, scale 1:24,000, https://doi.org/10.3133/gq144.
Snyder, G.L., 1964a, Bedrock geology of the Willimantic quadrangle, Connecticut: U.S. Geological Survey Geologic Quadrangle Map GQ-335, scale 1:24,000, https://doi.org/10.3133/gq335.
Snyder, G.L., 1964b, Petrochemistry and bedrock geology of the Fitchville quadrangle, Connecticut: U.S. Geological Survey Bulletin 1161-I, 63 p., 1 sheet, scale 1:24,000, https://doi.org/10.3133/b1161I.
Snyder, G.L., 1967, Bedrock geologic map of the Columbia quadrangle, east-central Connecticut: U.S. Geological Survey Geologic Quadrangle Map GQ-592, scale 1:24,000, https://doi.org/10.3133/gq592.
Snyder, G.L., 1970, Bedrock geologic map and magnetic maps of the Marlborough quadrangle, east-central Connecticut: U.S. Geological Survey Geologic Quadrangle Map GQ-791, scale 1:24,000, https://doi.org/10.3133/gq791.
Spear, F.S., and Harrison, T.M., 1989, Geochronologic studies in central New England I: Evidence for pre-Acadian metamorphism in eastern Vermont: Geology, v. 17, p. 181–184, https://doi.org/10.1130/0091-7613(1989)017<0181:GSICNE>2.3.CO;2.
Spear, F.S., Cheney, J.T., Pyle, J.M., Harrison, T.M., and Layne, G., 2008, Monazite geochronology in central New England: Evidence for a fundamental terrane boundary: Journal of Metamorphic Geology, v. 26, p. 317–329, https://doi.org/10.1111/j.1525-1314.2007.00751.x.
Stewart, E.M., and Ague, J.J., 2018, Infiltration-driven metamorphism, New England, USA: Regional CO_2 fluxes and implications for Devonian climate and extinctions: Earth and Planetary Science Letters, v. 489, p. 123–134, https://doi.org/10.1016/j.epsl.2018.02.028.
Stipp, M., Stünitz, H., Heilbronner, R., and Schmid, S.M., 2002, The eastern Tonale fault zone: A 'natural laboratory' for crystal plastic deformation of quartz over a temperature range from 250 to 700°C: Journal of Structural Geology, v. 24, p. 1861–1884, https://doi.org/10.1016/S0191-8141(02)00035-4.
Sutherland, R., et al., 2017, Extreme hydrothermal conditions at an active plate-bounding fault: Nature, v. 546, p. 137–140, https://doi.org/10.1038/nature22355.
Tikoff, B., and Teyssier, C., 1994, Strain modeling of displacement-field partitioning in transpressional orogens: Journal of Structural Geology, v. 16, p. 1575–1588, https://doi.org/10.1016/0191-8141(94)90034-5.
Tomascak, P.B., Krogstad, E.J., and Walker, R.J., 1996, U-Pb monazite geochronology of granitic rocks from Maine: Implications for late Paleozoic tectonics in the northern Appalachians: The Journal of Geology, v. 104, p. 185–195, https://doi.org/10.1086/629813.
Toy, V.G., Prior, D.J., and Norris, R.J., 2008, Quartz fabrics in the Alpine Fault mylonites: Influence of pre-existing preferred orientations on fabric development during progressive uplift: Journal of Structural Geology, v. 30, p. 602–621, https://doi.org/10.1016/j.jsg.2008.01.001.
Tullis, J., and Yund, R., 1992, The brittle-ductile transition in feldspar aggregates: An experimental study, *in* Evans, B., and Wong, T.-f., eds., Fault Mechanics and Transport Properties of Rocks: A Festschrift in Honor of W.F. Brace: London, Academic Press, International Geophysics, v. 51, p. 89–117, https://doi.org/10.1016/S0074-6142(08)62816-8.

Valley, P.M., Walsh, G.J., Merschat, A.J., and McAleer, R.J., 2020, Geochronology of the Oliverian Plutonic Suite and the Ammonoosuc Volcanics in the Bronson Hill arc: western New Hampshire, USA: Geosphere, v. 16, p. 229–257, https://doi.org/10.1130/GES02170.1.

van Staal, C.R., Whalen, J.B., Valverde-Vaquero, P., Zagorevski, A., and Rogers, N., 2009, Pre-Carboniferous, episodic accretion-related, orogenesis along the Laurentian margin of the northern Appalachians, *in* Murphy, J.B., Keppie, J.D., and Hynes, A.J., eds., Ancient Orogens and Modern Analogues: Geological Society, London, Special Publication 327, p. 271–316, https://doi.org/10.1144/SP327.13.

Vauchez, A., 1987, Brevard fault zone, southern Appalachians: A medium-angle, dextral, Alleghanian shear zone: Geology, v. 15, p. 669–672, https://doi.org/10.1130/0091-7613(1987)15<669:BFZSAA>2.0.CO;2.

Vauchez, A., Kessler, S.F., Lécorché, J.-P., and Villeneuve, M., 1987, Southward extrusion tectonics during the Carboniferous Africa–North America collision: Tectonophysics, v. 142, p. 317–322, https://doi.org/10.1016/0040-1951(87)90130-2.

Vermeesch, P., 2018, IsoplotR: A free and open toolbox for geochronology: Geoscience Frontiers, v. 9, p. 1479–1493, https://doi.org/10.1016/j.gsf.2018.04.001.

Vollmer, F.W., 1990, An application of eigenvalue methods to structural domain analysis: Geological Society of America Bulletin, v. 102, p. 786–791, https://doi.org/10.1130/0016-7606(1990)102<0786:AAOEMT>2.3.CO;2.

Vollmer, F.W., 1995, C program for automatic contouring of spherical orientation data using a modified Kamb method: Computers & Geosciences, v. 21, p. 31–49, https://doi.org/10.1016/0098-3004(94)00058-3.

Vollmer, F.W., 2024, Orient: Directional data analysis software: https://vollmerf.github.io/orient/ (accessed November 2024).

Waldron, J.W.F., Barr, S.M., Park, A.F., White, C.E., and Hibbard, J., 2015, Late Paleozoic strike-slip faults in Maritime Canada and their role in the reconfiguration of the northern Appalachian orogen: Tectonics, v. 34, p. 1661–1684, https://doi.org/10.1002/2015TC003882.

Waldron, J.W.F., McCausland, P.J.A., Barr, S.M., Schofield, D.I., Reusch, D., and Wu, L., 2022, Terrane history of the Iapetus Ocean as preserved in the northern Appalachians and western Caledonides: Earth-Science Reviews, v. 233, https://doi.org/10.1016/j.earscirev.2022.104163.

Walsh, G.J., Aleinikoff, J.N., and Wintsch, R.P., 2007, Origin of the Lyme dome and implications for the timing of multiple Alleghanian deformational and intrusive events in southern Connecticut: American Journal of Science, v. 307, p. 168–215, https://doi.org/10.2475/01.2007.06.

Walsh, G.J., Aleinikoff, J.N., Ayuso, R.A., and Wintsch, R.P., 2021, Age and tectonic setting of the Quinebaug-Marlboro belt and implications for the history of Ganderian crustal fragments in southeastern New England, USA: Geosphere, v. 17, p. 1038–1100, https://doi.org/10.1130/GES02295.1.

Walters, J.B., and Kohn, M.J., 2017, Protracted thrusting followed by late rapid cooling of the Greater Himalayan Sequence, Annapurna Himalaya, Central Nepal: Insights from titanite petrochronology: Journal of Metamorphic Geology, v. 35, p. 897–917, https://doi.org/10.1111/jmg.12260.

Walters, J.B., Cruz-Uribe, A.M., Song, W.J., Gerbi, C., and Biela, K., 2022, Strengths and limitations of in situ U–Pb titanite petrochronology in polymetamorphic rocks: An example from western Maine, USA: Journal of Metamorphic Geology, v. 40, p. 1043–1066, https://doi.org/10.1111/jmg.12657.

Wang, C., and Ludman, A., 2003, Evidence for post-Acadian through Alleghanian deformation in eastern Maine: Multiple brittle reactivation of the Norumbega Fault system: Atlantic Geology, v. 38, p. 32–52, https://doi.org/10.4138/1254.

West, D.P., and Hubbard, M.S., 1997, Progressive localization of deformation during exhumation of a major strike-slip shear zone: Norumbega fault zone, south-central Maine, USA: Tectonophysics, v. 273, p. 185–201, https://doi.org/10.1016/S0040-1951(96)00306-X.

West, D.P., and Lux, D.R., 1993, Dating mylonitic deformation by the ^{40}Ar-^{39}Ar method: An example from the Norumbega Fault Zone, Maine: Earth and Planetary Science Letters, v. 120, p. 221–237, https://doi.org/10.1016/0012-821X(93)90241-Z.

Williams, M.L., Jercinovic, M.J., Harlov, D.E., Budzyń, B., and Hetherington, C.J., 2011, Resetting monazite ages during fluid-related alteration: Chemical Geology, v. 283, p. 218–225, https://doi.org/10.1016/j.chemgeo.2011.01.019.

Wintsch, R.P., 1979, The Willimantic fault: A ductile fault in eastern Connecticut: American Journal of Science, v. 279, p. 367–393, https://doi.org/10.2475/ajs.279.4.367.

Wintsch, R.P., and Sutter, J.F., 1986, A tectonic model for the late Paleozoic of southeastern New England: The Journal of Geology, v. 94, p. 459–472, https://doi.org/10.1086/629051.

Wintsch, R.P., Sutter, J.F., Kunk, M.J., Aleinikoff, J.N., and Dorais, M.J., 1992, Contrasting P-T-t paths: Thermochronologic evidence for a Late Paleozoic final assembly of the Avalon composite terrane in the New England Appalachians: Tectonics, v. 11, p. 672–689, https://doi.org/10.1029/91TC02904.

Wintsch, R.P., Sutter, J.F., Kunk, M.J., Aleinikoff, J.N., and Boyd, J.L., 1993, Alleghanian assembly of Proterozoic and Paleozoic lithotectonic terranes in south-central New England; New constraints from geochronology and petrology, *in* Cheney, J.T., and Hepburn, T.C., eds., Field trip guidebook for the northeastern United States: University of Massachusetts, Department of Geosciences, Geosciences Contribution 67, v. 1, p. H-1–H-30.

Wintsch, R.P., Kunk, M.J., Boyd, J.L., and Aleinikoff, J.N., 2003, P-T-t paths and differential Alleghanian loading and uplift of the Bronson Hill terrane, south central New England: American Journal of Science, v. 303, p. 410–446, https://doi.org/10.2475/ajs.303.5.410.

Wintsch, R.P., Aleinikoff, J.N., Walsh, G.J., Bothner, W.A., Hussey, A.M., and Fanning, C.M., 2007, Shrimp U-Pb evidence for a Late Silurian age of metasedimentary rocks in the Merrimack and Putnam-Nashoba terranes, eastern New England: American Journal of Science, v. 307, p. 119–167, https://doi.org/10.2475/01.2007.05.

Wintsch, R.P., Yi, K., and Dorais, M.J., 2014, Crustal thickening by tectonic wedging of the Ganderian rocks, southern New England, USA: Evidence from cataclastic zircon microstructures and U–Pb ages: Journal of Structural Geology, v. 69, p. 428–448, https://doi.org/10.1016/j.jsg.2014.07.019.

Wintsch, R.P., Wathen, B.A., McAleer, R.J., Walters, J., and Matthews, J.A., 2024, Deformation by pressure solution and grain boundary sliding in a retrograde shear zone in southern New England, USA: American Journal of Science, v. 324, https://doi.org/10.2475/001c.125064.

Withjack, M., Malinconico, M., and Durcanin, M., 2020, The "passive" margin of eastern North America: Rifting and the influence of prerift orogenic activity on postrift development: Lithosphere, v. 2020, https://doi.org/10.2113/2020/8876280.

Zen, E.-a., Goldsmith, R., Ratcliffe, N.M., Robinson, P., Stanley, R.S., Hatch, N.L., Jr., Shride, A.F., Weed, E.G.A., and Wones, D.R., 1983, Bedrock geologic map of Massachusetts: U.S. Geological Survey, 3 sheets, scale 1:250,000.